https://dx.doi.org/10.1016/j.apenergy.2023.121770

Distributionally Robust Energy Management for Multi-Microgrids with Grid-interactive EVs Considering the Multi-period Coupling Effect of User Behaviors

Bifei Tan[a], Zhenjia Lin[b*], Xiaodong Zheng[c], Fu Xiao[b], Qiuwei Wu[d], Jinyue Yan[b]

[a] *Faculty of Intelligent Manufacturing, Wuyi University, Jiangmen 529000, Guangdong Province, China*
[b] *Department of Building Environment and Energy Engineering, The Hong Kong Polytechnic University, Hong Kong*
[c] *School of Electric Power, South China University of Technology, Guangzhou, 510641, China*
[d] *Tsinghua-Berkeley Shenzhen Institute, Tsinghua Shenzhen International Graduate School, Tsinghua University, Shenzhen, 518055, China*

ABSTRACT

The increasing penetration of renewable energy sources (RESs) in multi-microgrids (MMGs) poses significant challenges to stable operation of the systems, and exploring grid-interactive functionalities of electric vehicles (EVs) is receiving increasing attention. However, current distributionally robust energy management models suffer from convergence inefficiencies when exposed to large amounts of historical data, and typically neglect the multi-period coupling effect of EV user behaviors, which hinder the effective utilization of the highly-potential EV resources. In this paper, a novel distributionally robust energy management model for MMGs is proposed to accommodate the uncertainties of RESs and loads, with the grid-interactive EVs operating in an efficient vehicle-to-grid (V2G) mode. Firstly, a multi-period dynamic EV-connection matrix is formulated to determine the connection and dwell times for EVs interacting with the power systems, which enables the cross-cycle continuity of SOCs. Further, the multi-period coupling uncertainties of accidental EVs disconnections are taken into account. Secondly, the Kohonen neural network-based ambiguity set is constructed without including the entire historical scenarios, where the ambiguous distribution is characterized by the representative scenarios with weights. On this basis, a two-stage distributionally robust optimization model is finally developed, which can be solved iteratively by the extended column-and-constraint generation method until the worst-case cost expectation is obtained. The proposed model was evaluated through simulations on a system comprising four interconnected microgrids from the Hainan provincial power grid. The results demonstrate that the proposed model achieves superior cost efficiency, convergence performance and robustness compared to alternative approaches.

Keywords:
Distributionally robust optimization; Electric vehicle; Kohonen neural network; Multi-microgrids

Nomenclature

Abbreviations

MMG	Multi-microgrids
PV	Photovoltaic
WT	Wind turbine
DG	Diesel generator
PTDF	Power transmission distribution factor
FC	Fuel cell
ES	Energy storage
EV	Electric vehicle
LD	Load demand
UEV	Uncontrollable electric vehicle
EVA	Electric vehicle aggregator
SOC	State of charge
TP	Total number of connected EVs
IN	Number of EVs connecting
UN	Number of EVs disconnecting
SP	Sub-problem
MP	Master –problem
DR	Distributionally robust
KNN	Kohonen neural network

Parameters

$P_{\mathrm{WT},i}$	Predicted outputs of the *i*th WT unit
$c_{\mathrm{WT},j}$	Cost coefficient of the *i*th WT unit
$P_{\mathrm{PV,F}}$	Predicted output of the *i*th PV unit
$c_{\mathrm{PV},j}$	Cost coefficient of the *j*th PV unit
$c_{\mathrm{DG},j}$	Cost coefficient of the *i*th DG unit
$c_{\mathrm{FC},j}$	Cost coefficient of the *j*th FC unit
$c_j^{D/U}$	Shut down / start up cost coefficient of the *i*th DG unit
$C_i^{D/U}$	Shut down / start up cost of the *i*th DG unit
$P_{\mathrm{DG},i}^{\min/\max}$	Minimum / Maximum outputs of the *i*th DG unit
$P_{\mathrm{FC},i}^{\min/\max}$	Minimum / Maximum outputs of the *i*th FC unit
$P_{\mathrm{ES},i}^{\min/\max}$	Minimum / Maximum outputs of the *i*th ES unit
$P_{\mathrm{TL},i}^{\max}$	Maximum power transmission of the *i*th transmission line
$R_{\mathrm{ES},i}^{\mathrm{d/u}}$	Maximum downward/upward rate of the *i*th ES unit

* **Corresponding author.**
E-mail address: epjack.lin@polyu.edu.hk (Zhenjia Lin)

$R_{\mathrm{DG},i}^{\mathrm{d/u}}$	Maximum downward / upward rate of the *i*th DG unit
$R_{\mathrm{FC},i}^{\mathrm{d/u}}$	Maximum downward / upward rate of the *i*th FC unit
$\mathbf{P}_{i,r}$	Power flow distribution factor from node *i* to line *r*
$S_{\mathrm{EV}}^{'}$	SOC value of EV at the connection time
$S_{\mathrm{EV}}^{''}$	SOC value of EV at the disconnection time
$T_{\mathrm{IN},j}$	Connect time of *j*th EV
$d_{i,\mathrm{min/max}}$	Minimum / Maximum dwell time of EVs in *i*th EVA
$S_{\mathrm{EV}}^{\mathrm{min/max}}$	Minimum / Maximum SOC of an EV
$P_{\mathrm{load},\,i}$	Load power of the *i*th MG
$N_{\mathrm{TP},\,I}$	Number of EVs connected to the *i*th EVA
$N_{\mathrm{UP},i}^{*}$	Predicted number of EVs disconnected from *i*th EVA
$\mathbf{N}_{\mathrm{IN}}^{\mathrm{P}}$	Connection matrix of EVs of previous cycle
$\mathbf{N}_{\mathrm{IN}}^{\mathrm{D}}$	Connection matrix of EVs of current cycle
$\eta_{\mathrm{EV+/-},j}$	Charging / discharging efficiency of the *j*th EV
$c_{\mathrm{EV+/-},j}$	Cost coefficient of the charging/discharging power of EV at *j*th EVA
$T_{\mathrm{DG,O/S}}$	Minimum start-up / shut down times of DG
$P_{\mathrm{UEV},\,i}$	Charging power of a UEV
$P_{\mathrm{EV}}^{\mathrm{max}}$	Minimum / Maximum output of an EV
$R_{\mathrm{EV},i}^{\mathrm{d/u}}$	Maximum downward / upward ramping rate of EV at *j*th EVA
$B_{\mathrm{-L},i}$ / $B_{\mathrm{+L},i}$	Price of electricity purchase for the *i*th transmission line
$S_{\mathrm{-L},I}$ / $S_{\mathrm{+L},i}$	Price of electricity sale for the *i*th transmission line
$\mathfrak{I}$ / $\wp$ / $\mathbf{h}$	Unit sets
P	Ambiguity set
$\prod$ / Δ	Support set
$N_{\mu,1}/N_{\mu,2}/\omega_{ij}$	Training network parameters
Variables	
$\kappa/\varphi/\varepsilon$	Dual variables of the SP
$\boldsymbol{\mu}_i$	Uncertainty variable set
$P_{\mathrm{TL+/-},\,i}$	Forward/backward power transmission of the *i*th transmission line
$u_{\mathrm{TL},\,i}$	Operation index of the *i*th transmission line
$P_{\mathrm{DG},\,i}$	Output of the *i*th DG unit
$u_{\mathrm{DG},\,i}$	Operation index of the *i*th DG unit
$P_{\mathrm{FC},\,i}$	Output of the *i*th FC unit
$u_{\mathrm{ES},\,i}$	Operation index of the *i*th ES unit
$P_{\mathrm{ES},\,i}$	Transmission power of the *i*th ES unit
$P_{\mathrm{ES+/-},\,i}$	Positive/negative part of $P_{\mathrm{ES},\,i}$
$S_{\mathrm{ES},\,i}$	SOC of the *i*th ES unit
$\mathbf{U}_{\mathrm{IN},i}$	Uncertainty matrix of accidental disconnected EV of *i*th EVA
$t_j^{\mathrm{out/in}}$	Disconnection / connection time of the *j*th EV
$S_{\mathrm{EVA},\,i}$	SOC of the *i*th EVA
$P_{\mathrm{EVA+/-},\,i}$	Charging/discharging power of the *i*th EVA
$u_{\mathrm{EVA},j}$	Operation index of the *j*th EVA
$S_{\mathrm{EV},j,\,i}$	SOC of the *j*th EV at the *i*th EVA
$P_{\mathrm{EV+/-},j,\,i}$	Charging/discharging power of the *j*th EV at the *i*th EVA

I. Introduction

A. Motivation and Problem Statement

The proportion of distributed renewable energy sources (RESs) utilized in power systems has been increasing continuously in recent years. However, this trend will introduce challenges to currently available energy management system (EMS) because the operational status of RESs is vulnerable to weather, temperature, and other environmental factors, resulting in outputs that are characterized by randomness, intermittency, and volatility [1].

This issue can be potentially addressed via the rational use of microgrid systems that combine various locally distributed power sources, energy storage systems, and electrical loads with the main power grid, and thereby provide the flexibility for the energy systems [2,3]. The EMS of a microgrid can apply unit scheduling to make full use of the flexibility, economy, and environmental advantages of distributed energy sources and loads [4]. Moreover, the significant benefits of microgrids can be expanded by aggregating microgrids operating at the same hierarchical level to form multi-microgrid (MMG) clusters based on network structure and geographical distance [5].

In addition to the expansion of distributed RESs, the manufacturing and management of grid-interactive electric vehicles (EVs) are getting increasing attention worldwide. This rapid growth in market share has coincided with the concept of smart charging for the EVs, e.g., the vehicle-to-grid (V2G) mode, which can realize two-way power exchange between EVs and local grids, and therefore represents a novel and convenient distributed energy system [6]. The combined source and load profiles of EVs under the V2G architecture benefit both the power grid and the user side, and the proper management of EVs can have a comprehensive effect of stabilizing the power grid load, accommodating the uncertainties of RES outputs, and reducing network loss [7]. Meanwhile, the EVs user behaviors are becoming increasingly important, which have an impact on exploring the potential flexibility of EVs [8]. Therefore, it is of great necessity to develop the energy management model for MMGs with grid-interactive EVs, considering the coupling effect of user behaviors, so as to adapt to the uncertain environment with higher penetrations of RESs.

B. State-of-the Art Literature and limitations

In general, the uncertainty optimization problems have been solved using mainly stochastic optimization methods employing probability density functions (PDFs) obtained based on historical data [9][10][11], and robust optimization methods to establish uncertainty sets to obtain the worst-case scenarios [12][13]. Soykan *et al.* [9] proposed a two-stage stochastic programming-based multi-objective optimization model for determining the optimal configuration of an isolated microgrid. The uncertainties of RESs and loads are addressed by a scenario-based approach and the multi-objective problem is solved with the ε-constraint-based mathematical approach. Abunima *et al.* [10] proposed an artificial neural network-based prediction model to obtain the PDFs of RESs at each moment based on the historical data of their output range. Then, a two-stage stochastic optimization model is proposed to minimize the operating cost of a single islanded microgrid. Bagheri *et al.* [11] proposed a two-stage stochastic

programming model for the optimal sizing and operation of various distributed energy resources for peak load shaving in district buildings, and a generative adversarial network (GAN) was applied for generating the scenarios of uncertain parameters. Nevertheless, the PDFs of random variables are subjected to the predefined probability models and parameters, which will inevitably affect the results of stochastic optimization methods.

For the robust optimization, Guo *et al.* [12] designed an interval robust optimization (IRO) model to minimize the operation cost of an isolated microgrid, while considering the uncertainties set of RES outputs and industrial loads. The IRO problem was converted into a two-stage mixed-integer quadratic programming problem and the scheduling plan was then optimized for the worst-case scenario. Cheng *et al.* [13] proposed a robust decentralized energy management framework for the scheduling of a MMG system considering the uncertainties of RESs, heating loads and cooling loads. The maximum range of uncertainties is obtained from historical data, and intraday ultra-short-term optimal power allocation are obtained based on the RO strategy. Gilani *et al.* [14] proposes a two-phase method to elaborate a sustainable supply network design model for the solar photovoltaic supply chain. This work deals with the most significant concerns for policy-makers, that is, the uncertainties of radiation and demand parameters, by a data-driven robust (DDR) optimization model. However, robust optimization models tend to yield overly conservative solutions owing to the inclusion of unrealistic worst-case scenarios, resulting in unnecessarily high operating costs [15]. Besides, the construction of uncertainty set has a significant impact on the optimization results.

Table 1. Comparison of the characteristics of existing DRO considering EVs studies and the model proposed herein

	MMG		EVs			Uncertainty optimization		
Ref.	Number of regions	RESs uncertainty	Accommodation of RESs	Multi-period Coupling Effect of User Behaviors		Probabilistic analysis of uncertainty	Construction of uncertainty set	Improvement of ambiguity set
				Cross-cycle Continuity of SOCs	Multi-period coupling uncertainties			
[9]	Single	√	√		×	√	×	×
[10]	Single	√	×	×	×	√	×	×
[11]	Single	√	×	×	×	√	×	×
[12]	Single	√	√	×	×	×	IR	×
[13]	Single	√	×	×	×	×	IR	×
[14]	Multiple	√	×	×	×	×	DDR	×
[16]	Single	√	×	×	×	√	IRO/ DDR/DRO	×
[19]	Single	√	√	×	×	√	DDR/DRO	×
[20]	Multiple	√	×	×	×	√	DRO	×
[21]	Single	√	×	×	×	√	DDR/DRO	×
[22]	Single	√	√	×	×	×	IR	×
[23]	Single	√	×	×	×	√	×	×
[24]	Multiple	√	√	×	×	√	×	×
[25]	Single	×	×	×	×	√	×	×
[26]	Single	√	√	×	×	×	IR/ DDR	×
[27]	Multiple	√	×	×	×	×	IR/ DDR	×
Proposed	Multiple	√	√	√	√	√	IR/ DDR/DRO	KNN

The distributionally robust optimization (DRO) methods that combine the advantages of stochastic and robust optimization methods have recently been widely applied for solving EMS scheduling problems involving MMG systems. In contrast to the other methods, DRO aims to hedge against the worst-case distribution within the ambiguity set of the uncertainties [16]. Generally, the ambiguity sets adopted by DRO can be classified into two categories, i.e., the moment-based and distance-based ambiguity sets [17][18]. Traditional moment-based ambiguity sets only consider the first and second moment information, which could make overly pessimistic results due to the insufficient distribution information. As for distance-based DRO, it is difficult to theoretically determine the true distribution of uncertainties. However, the true distribution is certainly close to the empirical distribution of historical data, and the degree of closeness can be measured by statistical methods [19][20][21]. For example, Xu *et al.* [19] developed a continuous energy management model for MMG systems to manage the flexible/non-flexible demands of data centers and buildings. The uncertain characteristics of the electricity market price, energy demands, and renewable power production are controlled by the hybrid robust-stochastic model, among which the optimal cost with the maximum prediction deviation scenario can be obtained. Cao *et al.* [20] develop a DRO algorithm with ambiguity set based on Wasserstein distance. And it's applied to solve the transactive energy optimization problem with the uncertainties from real-time electricity price, renewable energy, loads, and electric vehicles. Li *et al.* [21] sought to alleviate the adverse effects arising from diverse uncertainties, including electricity demands, outdoor

temperature, the metabolism of occupants, and solar irradiance, by applying a bilayer model that made full use of historical data and managed the conservativeness of solutions. It's designed to calculate the worst-case cost expectation without requiring an exact probability distribution, which can effectively avoid the conservatism of scheduling solution. However, similar to stochastic optimization, the convergence performance of DRO methods is greatly affected by the size of the data set, and the credibility of the optimization results will be limited with the small sample size of data set. At the same time, the solution process of the distance-based DRO methods will fall into the "curse of dimensionality" when the sample size is large [18]. The above-mentioned DRO methods lack in-depth exploration of the processing of historical data, which suffer from convergence inefficiencies when exposed to large amounts of historical data.

As mentioned in Subsection A, the increasing EVs of MMG that can provide flexibility have great potential for accommodating the uncertainties of RESs and loads. Currently, there have been many studies on EV grid-connected models. Unlike the conventional distributed power generation or loads, the management of EVs relies on an EV aggregator (EVA) to connect a large number of individual EVs in specific areas and optimize the V2G process. However, existing EVA models are generally regarded as an integrated virtual battery with a continuously changing capacity [22]-[27]. Shi *et al.* [22] proposed an effective strategy to improve the security and economy of microgrid systems by modeling the uncertainties in the EV users' behavior, which is mathematically represented by the SOC of EVs as uncertainty prediction sets. And a charging / discharging model is proposed to improve the ability of EVs to accommodate the RESs. Zhang *et al.* [23] used a probabilistic sampling model to obtain the connection time and travel distance of disordered and ordered charging EVs, as well as the overall charging power profile of EVAs and their PDFs. Then, an optimization model was built to maximize the benefits of EV users. The tri-layer optimization framework proposed by Seyyedi *et al.* [24] accommodated uncertainties regarding electric loads, RES outputs, and EV users' charging demands using a bids-based method. Here, the PDF of the temporal number of grid-connected EVs is obtained by the Gauss equation, and simulation results showed that the participation of EVs in scheduling can lead to a cost reduction during peak hours. Wu *et al.* [25] considered aggregations of EVs and focused on uncertainties in the sampling results of the SOC of each EV at the time of its initial connection to the microgrid. On this basis, a two-layer model predictive control strategy was established for predicting the EV charging loads of a microgrid. Dai *et al.* [26] built a two-stage data-driven robust optimization model that considered the uncertainties in the outputs of RESs accommodated by EVA. The proposed shift-working V2G model provides beneficial characteristics, like weakened randomness and stable storage capacity. A quantitative method to evaluate the V2G capacity is then presented according to EV user behaviors. Tan *et al.* [27] applied an improved data-driven uncertainty set of RES and EVA with eliminated unrealistic worst-case scenarios. However, the above-discussed work models EVs according to their overall SOC and power, while ignoring the impact of the number of single EV connection events. Moreover, these researches have not taken into account the multi-period coupling effect of EV user behaviors, which hinder the effective utilization of the highly-potential EV resources.

C. Contributions

The characteristics of the main studies discussed above are summarized in Table 1. Here, the present work addresses the above issues by proposing a novel distributionally robust energy management model for MMG systems, like that illustrated in Fig. 1, where the grid-interactive EVs can operate in an efficient V2G mode with the multi-period coupling effect of user behaviors being taken into account. Also, the ambiguity set is improved by the introduction of the Kohonen neural network (KNN) to alleviate the convergence inefficiency of DRO. The main contributions of this work can be specified as follows.

(1) A novel distributionally robust energy management model is developed for MMG systems by effectively exploring the grid-interactive functionalities of EVs to accommodate the uncertainties of RESs and loads. The proposed model is an attempt for real case in the Hainan provincial power grid, which can make a better tradeoff between cost efficiency and robustness by hedging against the worst-case cost expectation.

(2) The multi-period coupling effect of user behaviors is characterized in this paper for a more elaborated modelling of gird-interactive EVs. Specifically, a multi-period dynamic EV-connection matrix determining the connection and dwell times for EVs is formulated to enable the cross-cycle continuity of SOCs. Also, the multi-period coupling uncertainties of accidental EVs disconnections are taken into account along with its quantitative mathematical models.

(3) The KNN-based ambiguity set is constructed to prevent the DRO from suffering convergence inefficiency when exposed to large amounts of historical data. The proposed ambiguity set preserves the properties of the entire historical scenarios through the weighted representative scenarios, which can be used to present the ambiguous distribution of random variables.

The remainder of this paper is organized as follows. Section II introduces the proposed MMG systems optimization models and analyzes the specific characteristics of uncertainties in the models. Section III presents the two-stage distributionally robust energy management model employing the KNN-based ambiguity set and describes the solution process using the extended column and constraint generation (C&CG) method, which is widely used to solve robust optimization problems. Section IV presents and discusses the results of numerical case studies. Finally, Section V concludes the paper with a report of its major findings.

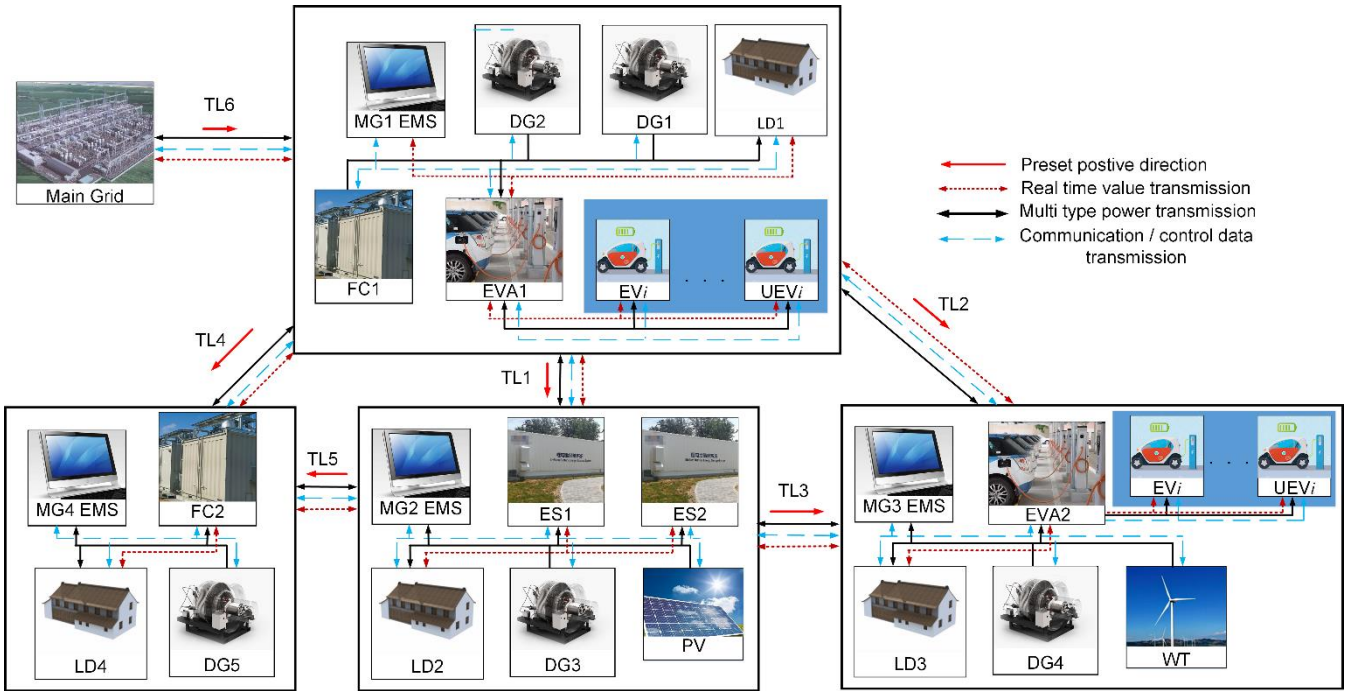

Figure 1. Network topology of a multi-microgrid system with transmission lines (TLs), diesel generators (DGs), fuel cells (FCs), electric loads (LDs), RESs, including PV and wind turbines (WTs), and EVs operating in a V2G mode.

II. Multi-microgrid model with grid-interactive EVs

2.1 Modeling of grid-interactive EVs Considering the Multi-period Coupling Effect of User Behaviors

In this section, the coupling effect of user behaviors is taken into account for the modelling of EVs to fully exploit the potential flexibility. As illustrated in Fig. 2, the coupling effect of user behaviors is further elaborated as the cross-cycle continuity of SOCs, i.e., Figs. 2(a) and (b), and the multi-period coupling uncertainties of accidental EVs disconnections in Fig. 2 (c), which will be specified in the following subsections.

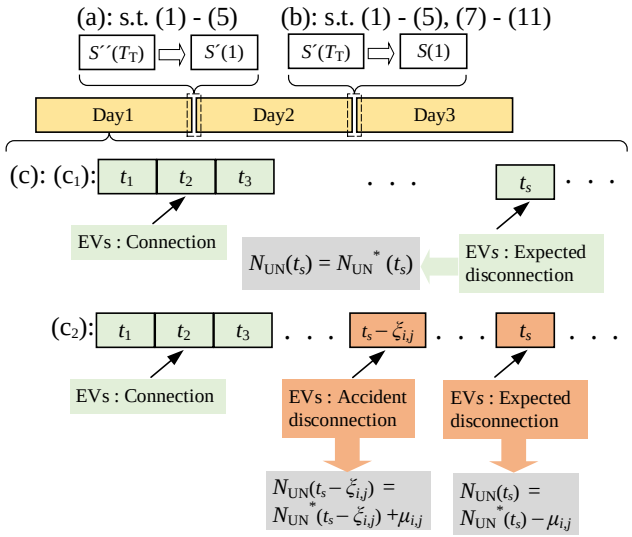

Figure 2. Multi-period Coupling Effect of User Behaviors: (a) Conventional EVA model; (b) The proposed EVA model; (c) Multi-period coupling mechanism of EV users' uncertainties

2.1.1 Modeling for EVs considering Cross-cycle Continuity of SOCs

The maximum rate of change in the power flow of an EVA can be related to the number of grid-connected EVs and the maximum rate of change in the power flow of a single EV. Therefore, the present work divides EVs into two categories, including (1) EVs that are connected with the power systems for durations (dwell times) that are too short for V2G to be approved and (2) EVs that are connected with the power systems for dwell times that are sufficient for the EV to serve as ES assets. All EVs adhering to category (1) are managed as pure loads when connected to the grid, while those adhering to category (2) are managed as ES units. Here, as displayed in Fig. 2 (a), the conventional EVA operates under the following constraints.

$$S_{\mathrm{EVA},i}(t+1)=\frac{P_{\mathrm{EVA}-,i}(t)\eta_{\mathrm{EV}-,i}-P_{\mathrm{EVA}+,i}(t)\eta_{\mathrm{EV}+,i}}{G_{\mathrm{EV}}}+S_{\mathrm{EVA},i}(t)+\sum_{j=1}^{N_{\mathrm{IN},i}(t)}S_{\mathrm{EV},j}-N_{\mathrm{UN},i}S_{\mathrm{EV}}^{"} \tag{1}$$

$$S_{\mathrm{EV},j}(t)=S_{\mathrm{EV},j}^{'},\forall t\le t_j^{\mathrm{in}},\ S_{\mathrm{EV},j}(t)=S_{\mathrm{EV}}^{''},\forall t\ge t_j^{\mathrm{out}}$$

$$\begin{cases}P_{\mathrm{EVA},i}(t)=P_{\mathrm{EVA}+,i}(t)-P_{\mathrm{EVA}-,i}(t)\\0\le P_{\mathrm{EVA}+/-,i}(t)\le u_{\mathrm{EVA},i}N_{\mathrm{TP},i}(t)P_{\mathrm{EV}}^{\max}\\0\le P_{\mathrm{EVA}-,i}(t)\le(1-u_{\mathrm{EVA},i})N_{\mathrm{TP},i}(t)P_{\mathrm{EV}}^{\max}\end{cases} \tag{2}$$

$$N_{\mathrm{TP},i}(t)S_{\mathrm{EV}}^{\min}\le S_{\mathrm{EVA},i}(t)\le N_{\mathrm{TP},i}(t)S_{\mathrm{EV}}^{\max} \tag{3}$$

$$\begin{cases}\tau_i R_{\mathrm{EV}}^{\mathrm{d}}N_{\mathrm{TP},i}(t)\le P_{\mathrm{EVA}-,i}(t+1)-P_{\mathrm{EVA}-,i}(t)\\P_{\mathrm{EVA}-,i}(t+1)-P_{\mathrm{EVA}-,i}(t)\le\tau_i R_{\mathrm{EV}}^{\mathrm{u}}N_{\mathrm{TP},i}(t)\\\tau_i R_{\mathrm{EV}}^{\mathrm{d}}N_{\mathrm{TP},i}(t)\le P_{\mathrm{EVA}+,i}(t+1)-P_{\mathrm{EVA}+,i}(t)\\P_{\mathrm{EVA}+,i}(t+1)-P_{\mathrm{EVA}+,i}(t)\le\tau_i R_{\mathrm{EV}}^{\mathrm{u}}N_{\mathrm{TP},i}(t)\end{cases} \tag{4}$$

$$S_{\mathrm{EV,D}}N_{\mathrm{UN},i}(t)+S_{\mathrm{EV,A}}(N_{\mathrm{TP},i}(t)-N_{\mathrm{UN},i}(t))\le S_{\mathrm{EV},i}(t) \tag{5}$$

Here, (1) represents the dynamic characteristics of the EVA, which are affected by its SOC at the previous moment, EV connection information, EV disconnection information, and the charge and discharge plan managed by the EMS. Constraints (2) and (3) are the upper and lower bounds between the charge

and discharge power of the EVA and the SOC. Constraint (4) limits the change in the EVA output. The power direction of EVs and EVAs is set positive when delivering power outward, i.e., $P_{\mathrm{EVA}+,i} > 0$. Otherwise, when the EVA is charged inward, $P_{\mathrm{EVA}-,i} > 0$ is true. Constraint (5) is introduced to ensure the sufficient SOC of EVs serving as ES units when disconnecting from the power grid. It is noted that for the ES units, the SOCs at the beginning and end of each scheduling cycle are consistent at the same fixed value, while there is no such consistency of the initial and final statuses for the EVA. As displayed in Fig. 2 (a), the cross-cycle continuity of SOCs for different days is neglected by the conventional EVAs, which may have an impact on user behaviors in the next scheduling cycle due to the insufficient SOCs of EV disconnected from the power grid. For example, there's an EV$_j$ in an EMS model with a T_{T}=24h scheduling time and 1h time resolution. Its connection time and dwell time are $t_j^{\mathrm{in}} = T_{\mathrm{T}} - d_j + t_\alpha$ and d_j, respectively. t_α is a positive integer indicating that EV$_j$ has a cross-cycle V2G process, that is, $t_j^{\mathrm{out}} = (t_j^{\mathrm{in}} + d_j) \geq T_{\mathrm{T}}$. Accordingly, the EMS cannot take into account the disconnection SOC constraint of EV$_j$ at the end of the current scheduling cycle ($t = T_{\mathrm{T}}$), thus the power of EV$_j$ is consumed as much as possible to replace the generation of high-cost thermal units, resulting in $S_{\mathrm{EV},j}(T_{\mathrm{T}}) \to S_{\mathrm{EV}}^{\min}$. As showed in (6), the SOC of EV$_j$ fails to reach the required value in disconnection time, which would further affect the user behaviors of EVs in the next scheduling cycle.

$$G_{\mathrm{EV}}(S_{\mathrm{EV}}'' - S_{\mathrm{EV},j}(T_{\mathrm{T}})) > P_{\mathrm{EV}}^{\max} t_\alpha \tag{6}$$

Therefore, it is necessary to consider the SOC of EVs related to the current scheduling cycle in the previous cycle. To address this, the following cross-cycle $(T_{\mathrm{T}} - d_{\min} + d_{\max}) \times (d_{\max} - d_{\min} + 1)$ element EV multi-period connection matrix is introduced.

$$\mathbf{N}_{\mathrm{IN}} = \left[\mathbf{N}_{\mathrm{IN}}^{\mathrm{P}} \middle| \mathbf{N}_{\mathrm{IN}}^{\mathrm{D}} \right] = \left[\begin{array}{cccc|ccc} \omega & \omega & \mathrm{L} & n'^{T_{\mathrm{T}}}_{d_{\min}} & n^1_{d_{\min}} & \mathrm{L} & n^{T_{\mathrm{T}}-1}_{d_{\min}} \; n^{T_{\mathrm{T}}}_{d_{\min}} \\ \mathrm{M} & \mathrm{M} & \mathrm{L} & n'^{T_{\mathrm{T}}}_{d_{\min}+1} & n^1_{d_{\min}+1} & \mathrm{L} & n^{T_{\mathrm{T}}-1}_{d_{\min}+1} \; n^{T_{\mathrm{T}}}_{d_{\max}} \\ \omega & n'^{T_{\mathrm{T}}-d_{\max}+2}_{d_{\max}-1} & & \mathrm{M} & \mathrm{M} & & \mathrm{M} \quad \mathrm{M} \\ n'^{T_{\mathrm{T}}-d_{\max}+1}_{d_{\max}} & n'^{T_{\mathrm{T}}-d_{\max}+2}_{d_{\max}} & \mathrm{L} & n'_{T_{\mathrm{T}},d_{\max}} & n^1_{d_{\max}} & \mathrm{L} & n^{T_{\mathrm{T}}-1}_{d_{\max}} \; n^{T_{\mathrm{T}}}_{d_{\max}} \end{array}\right] \tag{7}$$

Here, ω are the elements that are not be considered by the EMS in the current scheduling cycle, elements n'^{x}_{y} are the number of EVs connected to the power grid at time x with a dwell period of y hours in the previous scheduling cycle, and elements n^{x}_{y} represent the corresponding number of EVs that connected to the power grid at time x in the current scheduling cycle. Considering that the connection time $T_{\mathrm{IN},j}$ and dwell time d_j of different EVs are different, the total number N_{TP} of connected EVs and total number N_{UN} of EVs disconnecting at period t have the following relationship.

$$\begin{cases} N_{\mathrm{TP},i}(t+1) = N_{\mathrm{TP},i}(t) + \sum_{k=d_{\min}}^{d_{\max}} \mathbf{N}_{\mathrm{IN},i}^{\mathrm{D}}(t,k) - N_{\mathrm{UN},i}(t) \\ N_{\mathrm{UN},i}(t) = \sum_{n=1}^{¥} j_n, \quad ¥ = \left\{ j \mid T_{\mathrm{IN},j} + d_{d,j} = t \right\} \end{cases} \tag{8}$$

Meanwhile, N_{UN} has the following relationships with $\boldsymbol{N}_{\mathrm{IN}}$.

$$\begin{cases} N_{\mathrm{UN},i}(t_s) = \sum_{i=t_s+T_T-d_{\max}}^{t_s+T_T-d_{\min}} \mathbf{N}_{\mathrm{IN},i}^{\mathrm{P}}(t_s + T_{\mathrm{T}} - i, i), \quad \forall t_s \leq d_{\min} \\ N_{\mathrm{UN},i}(t_s) = \sum_{i=1}^{t_s-d_{\min}} \mathbf{N}_{\mathrm{IN},i}^{\mathrm{D}}(t_s - i, i), \quad \forall d_{\min} < t_s \leq d_{\max} \\ N_{\mathrm{UN},i}(t_s) = \sum_{i=t_s-d_{\max}}^{t_s-d_{\min}} \mathbf{N}_{\mathrm{IN},i}^{\mathrm{D}}(t_s - i, i), \quad \forall d_{\max} < t_s \leq T_{\mathrm{T}} \end{cases} \tag{9}$$

In addition, the connection time of connected EVs at the end of the current scheduling cycle (i.e., $t = T_{\mathrm{T}}$) is [$T_{\mathrm{T}} - d_{\min}$, $T_{\mathrm{T}} - d_{\max}$], which means that the EV elements surrounded by the trapezoidal region defined as $n^{T_{\mathrm{T}}-d_{\min}}_{d_{\min}+1} - n^{T_{\mathrm{T}}}_{d_{\min}} - n^{T_{\mathrm{T}}}_{d_{\max}} - n^{T_{\mathrm{T}}-d_{\max}+1}_{d_{\max}}$ have no effect on the value of N_{UN} for the entire scheduling period. Therefore, the convergence performance of the EV connection modeling process is improved by applying the following adjustment.

$$\mathbf{N}_{\mathrm{IN}} = \left[\begin{array}{ccccccccc} \omega & \omega & \mathrm{L} & n'^{T_{\mathrm{T}}}_{d_{\min}} & n^1_{d_{\min}} & \mathrm{L} & n^{T_{\mathrm{T}}-d_{\min}}_{d_{\min}} & \mathrm{L} & \omega \\ \mathrm{M} & \mathrm{M} & & n'^{T_{\mathrm{T}}}_{d_{\min}+1} & n^1_{d_{\min}+1} & \mathrm{L} & \omega & \mathrm{L} & \omega \\ \omega & n'^{T_{\mathrm{T}}-d_{\max}+2}_{d_{\max}-1} & & \mathrm{M} & \mathrm{M} & & \mathrm{M} & & \mathrm{M} \\ n'^{T_{\mathrm{T}}-d_{\max}+1}_{d_{\max}} & n'^{T_{\mathrm{T}}-d_{\max}+2}_{d_{\max}} & \mathrm{L} & n'_{T_{\mathrm{T}},d_{\max}} & n^1_{d_{\max}} & \mathrm{L} & \omega & \mathrm{L} & \omega \end{array}\right] \tag{10}$$

Therefore, as shown in Fig. 2 (b), the constraints of cross-cycle SOCs continuity (11) are included for the V2G process to avoid affecting the user behaviors of EVs in the next scheduling cycle, in particular those EVs disconnected at early periods.

$$\begin{cases} S_{\mathrm{EVA},i}(T_{\mathrm{T}}) \geq \sum_{l}^{d_{\min}} \sum_{k}^{T_{\mathrm{T}}} \left[\mathbf{N}_{\mathrm{IN}}(k,l) \left(S_{\mathrm{EV}}'' - \frac{(l+k-T_{\mathrm{T}}) P_{\mathrm{EV}}^{\max}}{G_{\mathrm{EV}}} \right) \right] \\ l,k \in \Upsilon, \quad \Upsilon = \left\{ (l,k) \mid l + k > T_{\mathrm{T}} \right\} \end{cases} \tag{11}$$

2.1.2 Modeling the multi-period coupling uncertainties of EVs

Based on the cross-cycle matrix $\mathbf{N}_{\mathrm{IN}}$, the multi-period coupling uncertainties of EVs is characterized by the number of accidental disconnections (i.e., earlier than the preset period) of EVs during the V2G process. As shown in Fig. 2, (c1) presents the expected scenario of EVs which connect at t_2, and disconnect at t_s ($n^2_{t_s-2}$ in (7)), while in the accidental scenario (c2), $\mu_{i,j}$ ($\mu_{i,j} \leq n^2_{t_s-2}$) presents the number of EVs that accidently disconnected at the time period ($t_s - \xi_{i,j}$). Accordingly, the number of disconnected EVs at t_s will decrease with the same $\mu_{i,j}$ due to the multi-period coupling effect. Here, it should be noted that the coupling uncertainties of EVs embody in the different time periods and the different number of EVs accidental disconnections. As a result, the characteristics of grid-interactive EVs are more clearly described by introducing the uncertainty of accidental disconnections as follows.

$$\begin{cases} N_{\mathrm{UN},i}(t)=N^{*}_{\mathrm{UN},i}(t), \quad \forall t \le (d_{\min}-1) \\ N_{\mathrm{UN},i}(t)=N^{*}_{\mathrm{UN},i}(t)+\sum\limits_{k=\max\{1,t-d_{\max}\}}^{t+\xi-d_{\min}} \mathbf{U}_{\mathrm{UN},i}(k,t+\xi_i-k-\delta_i) \\ \quad -\sum\limits_{k=\max\{1,t-d_{\max}\}}^{t-d_{\min}} \mathbf{U}_{\mathrm{UN},i}(k,t-k-\delta_i), \quad \forall(d_{\min,}-1)<t \\ \sum\limits_{t}^{T_T}\left|N^{*}_{\mathrm{UN},i}(t)-N_{\mathrm{UN},i}(t)\right| \le \Delta \end{cases} \tag{12}$$

Here, EVs with insufficient actual dwell time to participate in V2G are classified as uncontrollable EV loads if their actual dwell time is not more than half of a preset value because these EVs are not useful in peak shaving and RES absorption. The auxiliary index $\delta_i = d_{\min} - 1$ and the uncertainty matrix $\mathbf{U}_{\mathrm{UN}}(i, j) = \mu_{\mathrm{EV},i,j}$ are introduced. Each element of $\mathbf{U}_{\mathrm{UN}}$ represents the number of accidental disconnection of EVs in $\mathbf{N}^{\mathrm{D}}_{\mathrm{IN}}(i, j)$. In addition, the problem is formulated as follows to convert it into a mixed-integer linear programming (MILP) model.

$$\begin{cases} N_{\mathrm{UN},i}(t)=N^{*}_{\mathrm{UN},i}(t), \quad \forall t \le (d_{\min}-\xi_i) \\ N_{\mathrm{UN},i}(t)=N^{*}_{\mathrm{UN},i}(t)+\sum\limits_{k=1}^{t+\xi_i-d_{\min}} \boldsymbol{U}_{\mathrm{UN},i}(k,t+\xi_i-k-\delta_i), \\ \quad \forall(d_{\min}-\xi_i)<t \le d_{\min} \\ N_{\mathrm{UN},i}(t)=N^{*}_{\mathrm{UN},i}(t)+\sum\limits_{k=1}^{t+\xi_i-d_{\min}} \boldsymbol{U}_{\mathrm{UN},i}(k,t+\xi_i-k-\delta_i)- \\ \quad \sum\limits_{k=1}^{t-d_{\min}} \mu_{\mathrm{UN},i}(k,t-k-\delta_i), \forall d_{\min}<t \le (d_{\max}-\xi_i+1) \\ N_{\mathrm{UN},i}(t)=N^{*}_{\mathrm{UN},i}(t)+\sum\limits_{k=t+\xi_i-d_{\max}}^{t+\xi_i-d_{\min}} \boldsymbol{U}_{\mathrm{UN},i}(k,t+\xi_i-k-\delta_i)- \\ \quad \sum\limits_{k=1}^{t-d_{\min}} \boldsymbol{U}_{\mathrm{UN},i}(k,t-k-\delta_i), \forall(d_{\max}-\xi_i+1)<t<(d_{\max}+\xi_i) \\ N_{\mathrm{UN},i}(t)=N^{*}_{\mathrm{UN},i}(t)+\sum\limits_{k=t+\xi_i-d_{\max}}^{t+\xi_i-d_{\min}} \boldsymbol{U}_{\mathrm{UN},i}(k,t+\xi_i-k-\delta_i)- \\ \quad \sum\limits_{k=t-d_{\max}}^{t-d_{\min}} \boldsymbol{U}_{\mathrm{UN},i}(k,t-k-\delta_i), \forall(d_{\max}+\xi_i) \le t \\ \sum\limits_{t}^{T_T}\left|N^{*}_{\mathrm{UN},i}(t)-N_{\mathrm{UN},i}(t)\right| \le \Delta_i \end{cases} \tag{13}$$

Moreover, we note that the robust optimization model proposed in this paper must satisfy the SOC constraint (1) when an EV disconnects. Therefore, $\mathbf{N}_{\mathrm{IN}}$ can be incorporated into (13), and the problem converted into the following form.

$$\begin{cases} N_{\mathrm{UN},i}(t)=N^{*}_{\mathrm{UN},i}(t), \quad \forall t \le (d_{\min}-\xi_i) \\ \begin{cases} N_{\mathrm{UN},i}(t)=N^{*}_{\mathrm{UN},i}(t)+\mu_{\mathrm{EV},i}(t+\xi_i) \\ \mu_{\mathrm{EV},i}(t+\xi_i) \le \sum\limits_{k=1}^{t+\xi_i-d_{\min}} \mathbf{N}_{\mathrm{IN},i}(k,t+\xi_i-k-\delta_i), \\ \forall(d_{\min}-\xi_i)<t \le d_{\min} \end{cases} \\ \begin{cases} N_{\mathrm{UN},i}(t)=N^{*}_{\mathrm{UN},i}(t)+\mu_{\mathrm{EV},i}(t+\xi_i)-\mu_{\mathrm{EV},i}(t) \\ \mu_{\mathrm{EV},i}(t+\xi_i) \le \sum\limits_{k=1}^{t+\xi_i-d_{\min}} \mathbf{N}_{\mathrm{IN},i}(k,t+\xi_i-k-\delta_i) \\ \mu_{\mathrm{EV},i}(t) \le \sum\limits_{k=1}^{t-d_{\min}} \mathbf{N}_{\mathrm{IN},i}(k,t-k-\delta_i), \\ \forall d_{\min}<t \le (d_{\max}-\xi_i+1) \end{cases} \\ \begin{cases} N_{\mathrm{UN},i}(t)=N^{*}_{\mathrm{UN},i}(t)+\mu_{\mathrm{EV},i}(t+\xi_i)-\mu_{\mathrm{EV},i}(t) \\ \mu_{\mathrm{EV},i}(t+\xi_i) \le \sum\limits_{k=t+\xi_i-d_{\max}}^{t+\xi_i-d_{\min}} \mathbf{N}_{\mathrm{IN},i}(k,t+\xi_i-k-\delta_i), \\ \mu_{\mathrm{EV},i}(t) \le \sum\limits_{k=1}^{t-d_{\min}} \mathbf{N}_{\mathrm{IN},i}(k,t-k-\delta_i), \\ \forall(d_{\max}-\xi_i+1)<t<(d_{\max}+\xi_i) \end{cases} \\ \begin{cases} N_{\mathrm{UN},i}(t)=N^{*}_{\mathrm{UN},i}(t)+\mu_{\mathrm{EV},i}(t+\xi_i)-\mu_{\mathrm{EV},i}(t) \\ \mu_{\mathrm{EV},i}(t+\xi_i) \le \sum\limits_{k=t+\xi_i-d_{\max}}^{t+\xi_i-d_{\min}} \mathbf{N}_{\mathrm{IN},i}(k,t+\xi_i-k-\delta_i) \\ \mu_{\mathrm{EV},i}(t) \le \sum\limits_{k=t-d_{\max}}^{t-d_{\min}} \mathbf{N}_{\mathrm{IN},i}(k,t-k-\delta_i), \\ \forall(d_{\max}+\xi_i) \le t \end{cases} \\ \sum\limits_{t}^{T_T}\left|N^{*}_{\mathrm{UN},i}(t)-N_{\mathrm{UN},i}(t)\right| \le \Delta_i \end{cases} \tag{14}$$

2.2 Uncertainty modeling for RESs and loads

Generally, the uncertainties associated with the most common variables among microgrids, such as RESs, including PV and wind turbine (WT) units, and loads (LDs), which are also taken into accounted in this manuscript. In addition, considering that the IRO problem is more conservative than the DRO problem, an IRO model based on the boxed uncertainty set is developed to verify whether the proposed EVA model can adapt to the uncertainty of RES in the theoretical worst-case scenario. For the IRO model, uncertainty variables can be described by combinations of the predicted values and the corresponding volatilities [12], which are formulated as a box uncertainty set as follows.

$$\begin{cases} P_i(t)=P^{*}_i(t)+a^{+}_i(t)\mu^{+}_i(t)-a^{-}_i(t)\mu^{-}_i(t), \quad \forall i \in \pounds \\ \pounds=\{\mathrm{WT},\ \mathrm{PV},\ \mathrm{LD}\}, \\ \sum\limits_{t}^{T_T} a^{+}_i(t) \le \prod^{+}_i, \quad \sum\limits_{t}^{T_T} a^{-}_i(t) \le \prod^{-}_i \\ u^{+}_i(t) \le \Delta^{+}_i, \quad u^{-}_i(t) \le \Delta^{-}_i \end{cases} \tag{15}$$

Here, Δ^{+}_i and Δ^{-}_i are the maximum and minimum fluctuations of the i-th uncertain variable, respectively, which can be obtained from historical data and unit characteristics, and $\prod^{+/-}$ are the maximum numbers of maximum and minimum fluctuation scenarios in the model. We note here that, when $t = 0$, the variable converges to a deterministic variable, while the uncertainty of this variable reaches a maximum at $t =$

T_T. On the other hand, the uncertainty variables in DRO are generally described by the ambiguity set composed of the historical scenarios [28][29].

2.3 Robust energy management model for multi-microgrid systems

The robust energy management model is developed for the MMG systems, among which a robust scheduling solution involving grid-interactive EVs will be obtained to accommodate the uncertainties of RESs and loads. Accordingly, the controllable variables of the EMS appropriate to a MMG system are the outputs of diesel engine generators (DGs), fuel cells (FCs), ES units, connecting transmission lines (TLs), and controllable EVAs (Fig. 1). The optimization goal of the robust energy management model is to minimize the total cost G_T, which consists of the generation operation costs G_{OP} and transmission costs G_L that are defined as follows.

$$\begin{cases} G_T = G_{OP} + G_L, \\ G_{OP} = \sum_{t}^{T_T}\left[\sum_{j}^{N_{DG}}\left[C_j^U(t) + C_j^D(t)\right] + \sum_{\varepsilon}^{h}\sum_{j}^{N_\upsilon} c_{\varepsilon,j,t} P_{\varepsilon,j}(t)\right], \\ G_L = \sum_{t=1}^{T_T}\sum_{i,j\in L_B}^{L_B}\left[P_{i,j}(t)B_i(t) - P_{j,i}(t)B_j(t)\right], \\ h = \{DG, FC, ES, WT, PV, EVA-\} \\ C_i^D(t) \ge c_i^D\left(u_i(t-1) - u_i(t)\right), C_i^U(t) \ge c_i^U\left(u_i(t) - u_i(t-1)\right) \\ C_i^D(t) \ge 0, C_i^U(t) \ge 0 \end{cases} \tag{16}$$

The main constraints of the proposed model are given as follows.

$$\begin{cases} \sum_{k=t}^{t+T_{DG,O}-1} u_i(k) \ge T_{DG,O}\left(u_i(t) - u_i(t-1)\right) \\ \sum_{k=t}^{t+T_{DG,S}-1} \left(1 - u_i(k)\right) \ge T_{DG,S}\left(u_i(t-1) - u_i(t)\right) \end{cases} \tag{17}$$

$$\begin{cases} u_{DG,i}(t)P_{DG,i}^{min} \le P_{DG,i}(t) \le u_{DG,i}(t)P_{DG,i}^{max} \\ P_{FC,i}^{min} \le P_{FC,i}(t) \le P_{FC,i}^{max} \\ 0 \le P_{PV}(t) \le P_{PV,F}(t) \\ 0 \le P_{WT,}(t) \le P_{WT,F}(t) \\ -P_{ES-,i}^{max} \le P_{ES}(t) \le P_{ES+,i}^{max} \\ -P_{TL,i}^{max} \le P_{TL}(t) \le P_{TL,i}^{max} \end{cases} \tag{18}$$

$$\begin{cases} R_{DG,i}^{d} \le P_{DG,i}(t+1) - P_{DG,i}(t) \le R_{DG,i}^{u} \\ R_{FC,i}^{d} \le P_{FC,i}(t+1) - P_{FC,i}(t) \le R_{FC,i}^{u} \\ R_{ES,i}^{d} \le P_{ES,i}(t+1) - P_{ES,i}(t) \le R_{ES,i}^{u} \\ R_{TL,i}^{d} \le P_{TL,i}(t+1) - P_{TL,i}(t) \le R_{TL,i}^{u} \end{cases} \tag{19}$$

Here, (17) represents the start-up and shut-down time constraints of DGs, where $T_{DG,O}$ and $T_{DG,S}$ are the minimum start-up and shut-down times, respectively. The output value constraints of controllable variables are given in (18), while the ramping constraints of units are given in (19). In addition, binary variables $u_{ES/TL}$ are introduced as follows to reflect the fact that ESs and TLs cannot transmit forward and reverse power simultaneously in actual operation [28].

$$\begin{cases} P_{ES,i}(t) = P_{ES+,i}(t) - P_{ES-,i}(t) \\ 0 \le P_{ES+,i}(t) \le u_{ES,i}(t)P_{ES,i}^{max} \\ 0 \le P_{ES-,i}(t) \le (1 - u_{ES,i}(t))P_{ES,i}^{max} \\ P_{TL,i}(t) = P_{TL+,i}(t) - P_{TL-,i}(t) \\ 0 \le P_{TL+,i}(t) \le u_{TL,i}(t)P_{TL,i}^{max} \\ 0 \le P_{TL-,i}(t) \le (1 - u_{TL,i}(t))P_{TL,i}^{max} \end{cases} \tag{20}$$

$$S_{ES,i}(1) = S_{ES,i}(T_T) = 0.5 \tag{21}$$

$$S_{ES,i}(t+1) = S_{ES,i}(t) + P_{ES-,i}(t)\eta_{ES-,i} - P_{ES+,i}(t)\eta_{ES+,i} \tag{22}$$

Here, the power constraints of ES and TL are shown in (20), the SOC constraints of ESs in the scheduling cycle are given in (21) and (22). Finally, the power flow constraints of the proposed model are given succinctly as follows.

$$\begin{cases} \left|\sum_{j}^{\delta}\left(\sum_{\upsilon}^{\Im}\mathbf{P}_{j,r}P_\upsilon(t) - \sum_{\chi}^{\wp}\mathbf{P}_{j,r}P_\chi(t)\right)\right| \le P_{TL,r}^{max}, \\ \Im = \{DG, FC, ES, WT, PV, EVA, TL\}, \\ \wp = \{load, UEV\} \end{cases} \tag{23}$$

In addition, the power balance constraint of the MMG system is given as follows.

$$\begin{cases} \sum_{\upsilon}^{\Im} P_{\upsilon,t} = \sum_{\upsilon}^{\wp} P_{\upsilon,t}, \\ \Im = \{DG, FC, ES, WT, PV, EVA, TL\}, \\ \wp = \{load, UEV\} \end{cases} \tag{24}$$

III. Solution of the robust energy management model

In this paper, the C&CG algorithm adopts a main problem (MP) and a subproblem (SP) in the solution process. The uncertainty set is transformed into optimization constraints in the robust optimization process through McCormick envelope relaxation [30][31]. All details regarding the specific iteration process employed herein have been previously reported [26]. Briefly, the solution process determines whether worst-case scenarios are included in the uncertainty set in the SP, and constraints and new variables are added to the MP. The current solution remains the optimal solution for the worst-case scenario in the uncertainty set until the results of the MP and the SP differ by a specified amount.

3.1 Distributionally robust optimization

As discussed, the solutions obtained from robust optimization will tend to be overly conservative because the solution must be feasible under the possibility that $\prod = T_T$ in formula (15), even though this possibility is very small in practice. This issue can be addressed by applying the Wasserstein distance (W) based on the difference between the distributions of scenarios based on historical data. Specifically, we consider the distribution formed by the scenario set as the center of a sphere with a radius of W, and all distributions within that sphere serve as the ambiguity set, which can be observed from the original scenario set. Theoretically, the worst-case distribution of uncertainty variables is assured of being included in the sphere as long as the value of W is reasonable. Thereby, the solutions and cost expectation of the DRO model can be obtained.

The Wasserstein distance is often used to calculate the difference between two completely non-coincident

distributions P_1 and P_2, where the differences between the distributions increase with increasing $W(P_1, P_2)$ according to the following definition.

$$W(P_1, P_2) = \inf_{S(P_1,P_2)} \left\{ E_{S(P_1,P_2)} \left[d\left(\boldsymbol{\mu}_1, \boldsymbol{\mu}_2\right) \right] \right\} \quad (25)$$

Here, inf is the maximum lower bound, $S(P_1, P_2)$ represents all possible joint distributions between P_1 and P_2, and the term $\{\cdot\}$ within braces represents the expectation of the distance between the respective values ($\boldsymbol{\mu}_1$ and $\boldsymbol{\mu}_2$) of P_1 and P_2.

Accordingly, we can define the general robust optimization model as follows.

$$\mathbf{MP}: \quad \min_{\boldsymbol{x}} \mathbf{A}\boldsymbol{x} + \Psi \quad (26)$$

$$\text{s.t.} \quad \Lambda = \begin{cases} \Psi \geq \mathbf{B}\boldsymbol{y}, \mathbf{F}\boldsymbol{x} \geq \mathbf{f}, \mathbf{G}\boldsymbol{y} \geq \mathbf{g}, \\ \mathbf{U}\boldsymbol{y} + \mathbf{V}\boldsymbol{\mu} = \mathbf{w}, \mathbf{C}\boldsymbol{x} + \mathbf{D}\boldsymbol{y} \geq \mathbf{d} \end{cases} \quad (27)$$

Here, **A**, **B**, **F**, **f**, **G**, **g**, **U**, **V**, **C**, and **D** are the parameter matrices of the actual model, $\boldsymbol{x}$ is the binary variable of the first stage, $\boldsymbol{y}$ is the non-negative variable of the second stage, and $\boldsymbol{\mu}$ is the vector of uncertainty variables whose distributions are described in the ambiguity set. (26) is a compact expression of the overall operating cost objective function illustrated in Section II, and (27) is the operating constraints of each element of the MMG, such as the ramping constraint, the power output constraints, the SOC variation characteristics, etc..

$$\min_{\boldsymbol{x}} \{ \max_{P \in \mathbb{P}} \mathbf{A}\boldsymbol{x} + E_P[\Psi(\boldsymbol{x}, \boldsymbol{\mu})] \} \quad (28)$$

Here, (28) shows the cost expectation of MMG under the worst-case distribution of $\boldsymbol{\mu}$ in the DRO model.

The second part is the expectation of continuous variable operation cost, which is an infinitely dimensional continuous linear problem. The unit startup and shutdown decision in the first stage is updated by solving the second stage problem and constructing the extremal distribution. For a model with multiple uncertainties, it can be rewritten as follows.

$$\max \int_i \Psi(\boldsymbol{x}, \boldsymbol{\mu}) f_i d P_i \quad (29)$$

$$\text{s.t.} \quad P_{\mu} \in \mathbb{P} \quad (30)$$

$$\int_{\mu} \left\| \boldsymbol{\mu} - \boldsymbol{\mu}_k \right\|_1 f_{\mu} \, d P_{u,i}, \max_{P \in \mathbb{P}} (W(P, \mathbb{P}_k)) \quad (31)$$

Here, (31) ensures that the solution provided by the distributionally robust model can satisfy all scenarios in the ambiguity set. The MP defined above is used to obtain the optimal economic cost M_1 and $\boldsymbol{x}^*$ of the current distribution scenario, and then M_1 and $\boldsymbol{x}^*$ are transmitted to the following SP.

$$\mathbf{SP}: \max_{\mathbf{v}} \mathbf{g}^{\mathrm{T}} \kappa - (\mathbf{C}\mathbf{x} - \mathbf{d})^{\mathrm{T}} \varphi - (\mathbf{V}\mathbf{v} - \mathbf{w})^{\mathrm{T}} \varepsilon \quad (32)$$

$$\text{s.t.} \ \mathbf{B}^T - \left(\mathbf{G}^T \kappa + \mathbf{D}^T \varphi + \mathbf{U}^T \varepsilon \right) = 0, \kappa, \varphi, \varepsilon \geq 0 \quad (33)$$

This process provides the solution M_2 of the dual problem, which is employed in conjunction with M_1 and a predetermined convergence error value e, where, if $\frac{M_1 - M_2}{M_2} < e$ is not true, return the expected $\boldsymbol{y}^*$ to the MP, and update the constraint Λ. Otherwise, the convergence condition has been reached, and the current distribution is the worst-case distribution.

3.2 KNN based-ambiguity set

The distributionally robust method discussed above, which uses the Wasserstein distance, is prone to a significant increase in dimensionality if an empirical distribution with a large number of historical scenarios is employed. This can lead to computational challenges due to the convergence inefficiencies. Moreover, the characteristics of the original dataset must be preserved as much as possible in the scenario reduction process. This preservation can be ensured via a very simple and intuitive way according to the difference in the area or shape between the reduced scenario set and the original dataset. Kohonen neural network (KNN) is a type of artificial neural network that comprises of a topological 2D-lattice of neurons with each neuron capable of quantizing the input vectors to low-dimensional weight vectors. The basic principle behind the KNN is to transform the high-dimensional input vectors into lower-dimensional topology using an unsupervised winner-take-all competitive learning procedure. The uncertainty variables considered in this paper include WT, PV, LD, and EVA, resulting in an ambiguity set with lots of dimensions. Compared with other prediction or clustering-based neural network methods, e.g., Convolutional Neural Network (CNN), Recurrent Neural Network (RNN), Multilayer Perceptron (MLP), Receptive field (RF), Busy Lamp Field (BLF), the multi-dimensional topology-based KNN can cluster scenarios from a high-dimensional perspective, enabling the identification of features that distinguish between different scenarios. Therefore, this paper applies the KNN-based scenario reduction method to construct the ambiguity set.

1) Conventional probability distance-based scenario reduction

Data preprocessing is first applied to obtain a subset of the initial scenario set in which the probabilities of each scenario are equal. Then, the Euclidean distances between all scenarios are fashioned into a matrix $\boldsymbol{\theta}$ to obtain the two scenes with the closest nonzero distance. This work generates a new scenario along with its probability from these two scenarios, and the reduced scenario set is obtained after multiple iterations.

An example of the reduction in the scenario set for an uncertain variable μ_1 is presented in Fig. 3. For a scenario set with Z scenarios, the Euclidean distance between each scenario is calculated according to the following formula.

$$\theta_{i,j} = \begin{cases} 0, & i = j \\ \left\| \boldsymbol{S}_i - \boldsymbol{S}_j \right\|_2, & i \neq j \end{cases} \quad i, j \in Z \quad (34)$$

Then, the scenario with the smallest Euclidean distance in the matrix $\boldsymbol{\theta}$ is removed, and the scenario S_a with the closest Euclidean distance to that of the omitted scenario $S_b$is applied to generate a new scenario S_a' as follows:

$$P(S_a^{'}) = \lambda P(S_b) + P(S_a) \quad (35)$$

where λ is the probability redistribution coefficient. This process of omitting the scenario with the smallest Euclidean distance and generating a new scenario is continued until the number of scenarios is reduced to the set value, which is determined by the original data volume and the performance of the computing platform. In this respect, as shown in Fig. 3, the number of scenarios in the reduced scenario set of (b) can be significantly reduced while the properties of data can be well preserved. On the contrary, the initial scenario set of (a) contains the large number of historical scenarios, which imposes a computational burden for solving the DRO model.

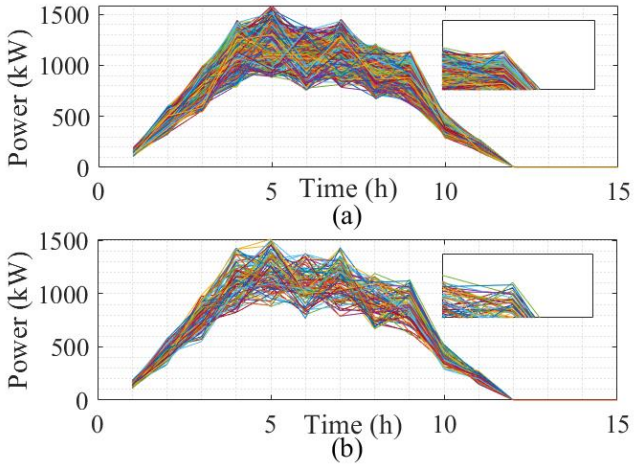

Figure 3. Reduction of the scenario set for uncertain variable u_1: (a) initial set; (b) reduced set.

2) Kohonen neural network

The first layer of a Kohonen neural network structure is the input layer, and the number of nodes ($N_{\mu,1}$) in this layer is consistent with the dimension of the input sample vector. The second layer is the competition layer, also known as the output layer, and its nodes are distributed in a two-dimensional (2D) array. The total number of nodes in the competition layer is defined as $N_{\mu,2}$, so the network weights are defined as ω_{ij} (i = 1, 2, …, $N_{\mu,1}$, j = 1, 2, …, $N_{\mu,2}$). The distance between the nodes is defined according to the input sample μ_i and the weight ω_{ij} as follows.

$$d_j = \sum_{i=1}^{N_{\mu,1}} (\mu_i - \omega_{ij})^2 \quad j = 1,2,\mathrm{L}\ ,N_{\mu,2} \tag{36}$$

When a normalized sample is input into the Kohonen neural network, a neuron on the competitive layer calculates the distance between the input sample and the weight of the neuron on the competitive layer. The weights of the neuron with the smallest distance and its neighbors (i.e., neurons whose distance from this neuron is less than the set domain radius) are adjusted as follow.

$$\omega_{ij} = \omega_{ij} + \eta(\mu_i - \omega_{ij}) \tag{37}$$

to make these weights close to the input sample for conducting the repeated weight training process of competition layer neurons according to a previously published process [33][34]. Finally, the connection weights of each neuron in the competition layer develop a particular distribution, which is illustrated for an arbitrary case in Fig. 4.

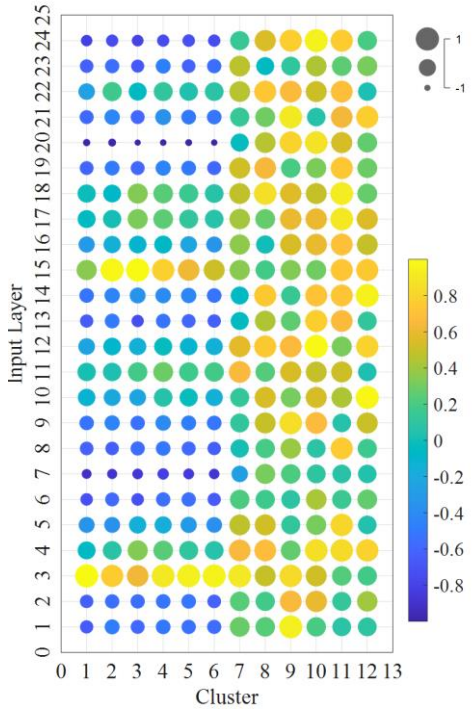

Figure 4. Illustrative weight distribution for a 24-node input layer and 12 nodes in the competition layer

Some research work in obtaining representative scenarios of clusters based on average values leads to positive and negative biases offsetting each other. To avoid the loss of scenario information in the process of clustering, which can affect the robustness of the model, this paper combines the framework in (38) with the Wasserstein distance as follows:

$$\max \left| \frac{\boldsymbol{S}_{\mathrm{AG}} - \boldsymbol{S}^*}{\boldsymbol{S}^*} \right| \geq \Delta - \delta \tag{39}$$

to form test conditions in the selection of representative scenarios, where δ is the minimum robustness tolerance value. As a result, the KNN based-ambiguity set can be yielded with the weighted representative scenarios, and thereby avoid the large number of historical scenarios employed in conventional empirical distributions. New MP and SP are derived by importing the scenarios obtained by the proposed scenario reduction and clustering processes into (28), as reported in a previous study [18].

3.3 Solution process

Based on the discussion in this section, the specific steps employed for the two-stage DRO energy management of MMG systems are given as follows.

Step 1: Preprocess the historical data by cutting and merging scenarios according to the Euclidian distance until a pre-established number of scenarios has been obtained.

Step 2: Initialize the Kohonen neural network and cluster the preprocessed data until convergence. If (39) is true, go to Step 3; otherwise, return to Step 1.

Step 3: Initialize the distributionally robust optimization process by setting the upper bound in the SP as $M_2 = +\infty$, the lower bound in the **MP** as $M_1 = -\infty$, and the iteration index as $\upsilon = 0$. Obtain the range of parameter values like $S_{\mathrm{EVA},i}$ and $N_{\mathrm{TP},i}$ in the first period according to the scenario data.

Step 4: The binary variable $\boldsymbol{x}^{\upsilon}$ and lower bound M_1^{υ} are obtained in iteration v by solving the minimum operation cost

of the current selected distribution scenario, which is the deterministic scenario when $\upsilon = 0$.

Step 5: Pass $\boldsymbol{x}^{\upsilon}$ to the SP.

Step 6: A variety of distribution scenarios and their probability weights are constructed in the SP according to the scenario data, and the SP is solved to obtain the values of the continuous variables $\boldsymbol{y}^{\upsilon}$ and the upper bound M_2^{υ} in iteration v.

Step 7: The process is terminated if $\frac{M_1 - M_2}{M_2} < e$, and the final results are output. Otherwise, add the selected distribution scenario to Λ, set $v = v + 1$, and return to Step 5.

IV. Demonstrative case study

4.1 Description

The test system from the Hainan, China [35] employed herein for demonstrating the applicability of the proposed optimization model is that illustrated in Fig. 1, which consists of four interconnected microgrids, two EVAs, and various units employed within each microgrid. The specific components of the test system are described in Table 2. Based on a comprehensive analysis of existing studies [36][37], the maximum deviation of RES outputs applied in the present work when constructing the box uncertainty set was assigned as ±30% of its predicated output. In addition, the maximum deviation of the load was set as ±15% of its predicated demand.

Table 2. Unit information of the multi-microgrid system (Fig. 1) employed herein for testing

Unit	Capacity (kW)
DG1, DG2, DG3	5100, 5400, 6150
DG4, DG5	5100, 3600
FC1, FC2	3500, 3300
ES1, ES2	1520, 1850
PV, WT	400, 1200
L1, L2, L3	2300
L4, L5, L6	

More specifically, each microgrid uses a different three-stage TOU pricing strategy based on local conditions. In addition, the load curves of LD1–LD4, respectively, applied for microgrids MG1–MG4 in the simulations are presented in Fig. 5 at a temporal resolution of one hour. We note that the load of MG4 is considerably greater than the other loads owing to a high local industrial electric load. The simulations applied herein considered 24 hourly time points within the scheduling period of a single day. The EV connection data obtained according to the historical data of EVAs is presented in Fig. 6 with connection times running from 3:00 to 2:00 the next day at a temporal resolution of one hour. The maximum dwell time ($d_{\max}$) and minimum dwell time ($d_{\min}$) for an EV was connected to the grid were 14 h and 6 h, respectively. Besides, the SOC of each EV is indicated by color according to the color scale provided.

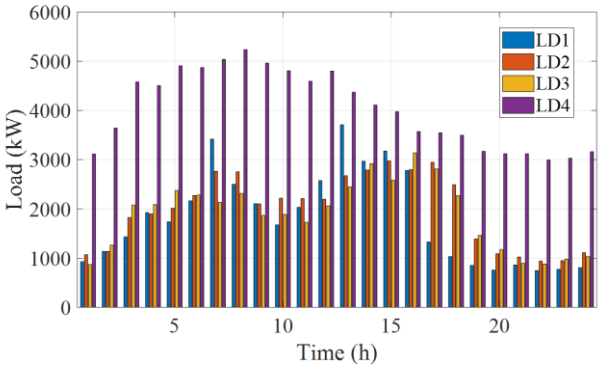

Figure 5. Load curves of the multi-microgrid system

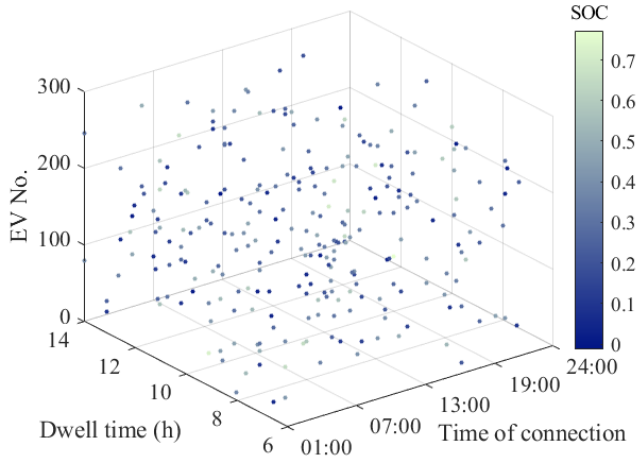

Figure 6. EVs connection data of the multi-microgrid test system

All numerical simulations were conducted using MATLAB with the YALMIP toolbox operating on a personal computer running Windows 10 with a 4-core 2.6 GHz CPU and 16 GB of memory.

To illustrate the effectiveness of the proposed DRO energy management model for MMG systems, the four cases listed in Table 3 are thoroughly studied, which are set as follows:

Case 1: The branch and bound (B&B) algorithm [38], C&CG, DRO method and the improved method are tested on the MMG systems, and the uncertainty is characterized by the deterministic scenario. It is noted that the consistency and stability of the model can be assured when the various methods in the test case converge to the same optimal operating cost. Case 1 corresponds to those potential cases that the forecast information on uncertain variables is available to the system operator.

Case 2: This case is presented to verify the effectiveness and economy of the proposed EVA model for the theoretical worst-case scenario. All uncertain variables in IRO model are represented by the box uncertainty set. The C&CG algorithm is applied for the robust optimization problem to obtain the optimal operating cost for the worst-case scenario in the box uncertainty set. In contrast to the deterministic optimization, Case 2 corresponds to those potential cases that only the uncertain range of variables are available to the system operator.

Case 3: All uncertain variables are characterized by their distributions of the non-clustered ambiguity set, and the C&CG method is used for solving the DRO energy management model. It is noted that the ambiguity set based on the distribution characteristics of historical scenario data avoids theoretically existing but extreme scenarios, and therefore avoids overly conservative solutions. Case 3 corresponds to those potential

cases that the historical scenarios as well as the forecast information on uncertain variables is available to the system operator.

Case 4: All uncertain variables are characterized by their distributions of the KNN-based ambiguity set, and the extended C&CG method is used for solving the DRO energy management model. By comparing the results obtained for Cases 3 and 4, the superiority of the proposed ambiguity set construction method can then be demonstrated. Similar to Case 3, Case 4 corresponds to those potential cases that the historical scenarios as well as the forecast information on uncertain variables is available to the system operator.

Table 3. Information regarding the four case studies employed for testing.

Index	Method	Consideration
Case 1	B&B	Deterministic scenario
	C&CG	
	DRO method	
	Improved DRO method	
Case 2	C&CG	Box uncertainty set
Case 3	DRO method	Non-clustered ambiguity set
Case 4	Proposed	KNN-based ambiguity set

4.2 Analysis of specific case results

Case 1

The operating costs obtained by the various methods applied for the deterministic scenario in Case 1 were uniformly 118418 yuan. This uniformity occurred because $\mu = 0$ for the deterministic scenario, McCormick envelope relaxation cannot affect the model constraints, and the SP is a strong dual problem of the MP $M_1^1 = M_2^1$, making the C&CG solution equivalent to that of the B&B algorithm in the very first iteration. Similarly, the same solution is obtained by the DRO and improved DRO methods because the ambiguity set converges to the same single deterministic scenario. Accordingly, the results demonstrate the consistency and stability of the proposed model.

The operation schedule of the thermal units, energy storage, and transmission lines obtained under the deterministic scenario are shown in Figs. 7(a), (b), and (c), respectively. As can be seen in Fig. 7(a), the DGs produce most of the active power due their low costs, but this factor varies greatly according to the load variation characteristics of different regions. For example, the output of DG5 operating in MG4 is nearly constant throughout the entire day (1:00–13:00) to meet locally high loads (Fig. 5), and a rapid increase in the generation of DGs is observed only later when LD2 increases to a maximum value again at 15:00. In addition, FC units with higher cost and more flexible start-up scheduling are mainly used to provide power over short periods when RESs and load fluctuates violently. We further note from Fig. 7(b) that the two ES units in MG2 generally take advantage of the low load during the night to store energy at that time to prepare for the high load demands in the daytime. Hence, the MMG system realizes the redistribution of loads from peak-load periods to low-load periods. Moreover, we note that the flow direction of power for ES2 changes earlier than that of ES1 owing to its higher rate of change. Overall, considering the high stability of the system in the deterministic scenario, the power fluctuation of each unit and transmission line is small.

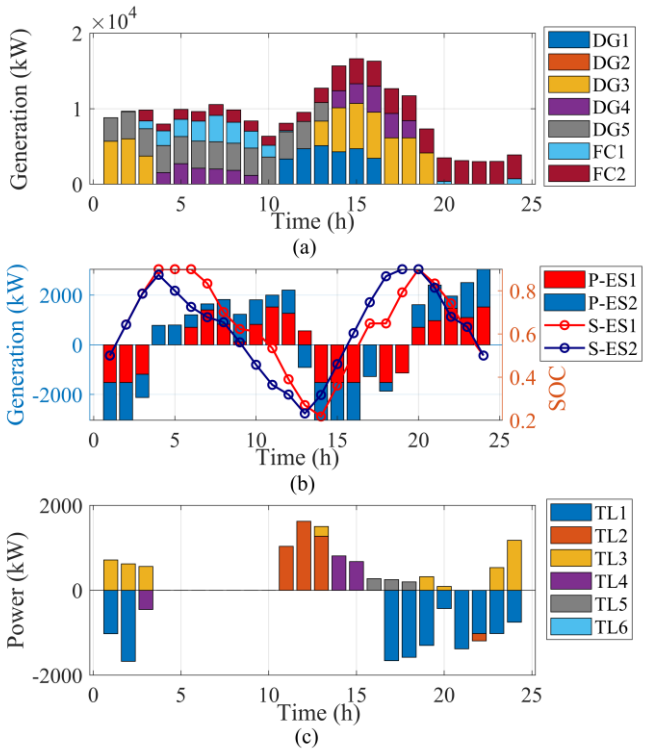

Figure 7. Outputs of main units under the deterministic scenario (Case 1): (a) thermal power units; (b) ES units; (c) TLs.

A full understanding of the transmission lines shown in Fig. 7(c) requires the presentation of the power flows and overall SOCs of EVA1 operational in MG1 and EVA2 operational in MG3, which are, respectively, given by the bar and line graphs in Fig. 8(a).

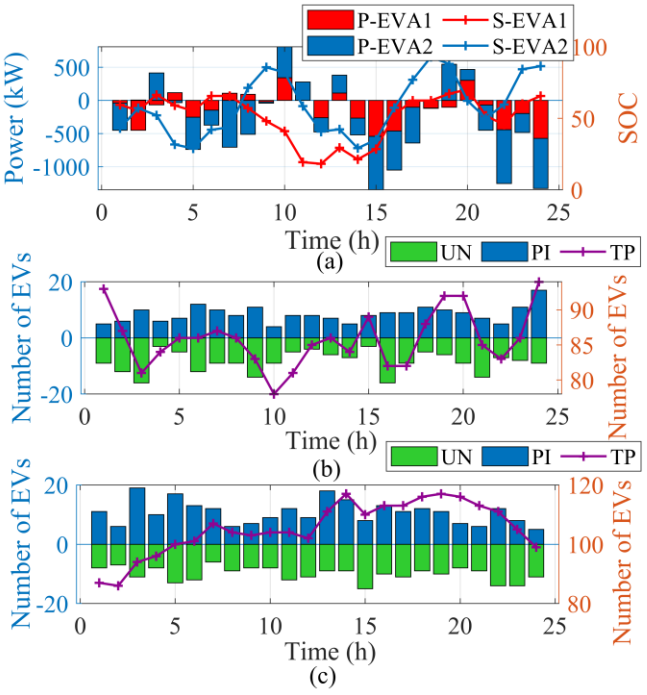

Figure 8. Scheduling solutions of EVAs under Case 1: (a) power flows and SOCs of EVAs; (b) number of EVs connecting to EVA1.

A comparison of Figs. 7(c) and 8(a) indicates that MG1 and MG3 require electrical power from external sources to meet the local EVA charging loads in the daytime and at night. The colors of the points plotted in Fig. 6 indicate that many EVs have a low SOC when they are connected to an EVA. Therefore,

Fig. 8(a) shows that the EVAs require power supplied to them most of the time to accommodate EV charging operations. However, both EVAs become a source of power to the outside at around 10:00, 13:00, and 20:00, which verifies that EVs operating in a V2G setting can provide energy storage services for a MMG system. We also present the number of EVs connecting to EVA1 and EVA2 in Figs. 8(b) and (c), respectively, where UN is the number of EVs disconnecting, PI is the number of EVs connecting, and TP is the total number of EVs connected to the EVA at the selected time. As for Figs. 8(b) and (c), the left y-axis corresponds to UN and PI, and the right y-axis corresponds to TP, which illustrates the EV temporal connection situations of EVAs. As can be seen, EVA2 has a larger number of EVs connected to the microgrid than EVA1, and the number fluctuates slightly. Therefore, EVA2 has a larger charge/discharge power and better energy flexibility than EVA1 while meeting off-grid EV SOC constraints (40) and (41).

Case 2

The outputs of the thermal power units, power flows and SOCs of ES units, and the power flows of TLs obtained under Case 2 are presented in Figs. 9(a), (b), and (c), respectively. The optimal operating cost obtained under Case 2 was 142597 yuan, which is 20.42% greater than that obtained under the deterministic scenario. Theoretically, this arises because the load under the worst-case scenario is generally greater than that of the deterministic scenario.

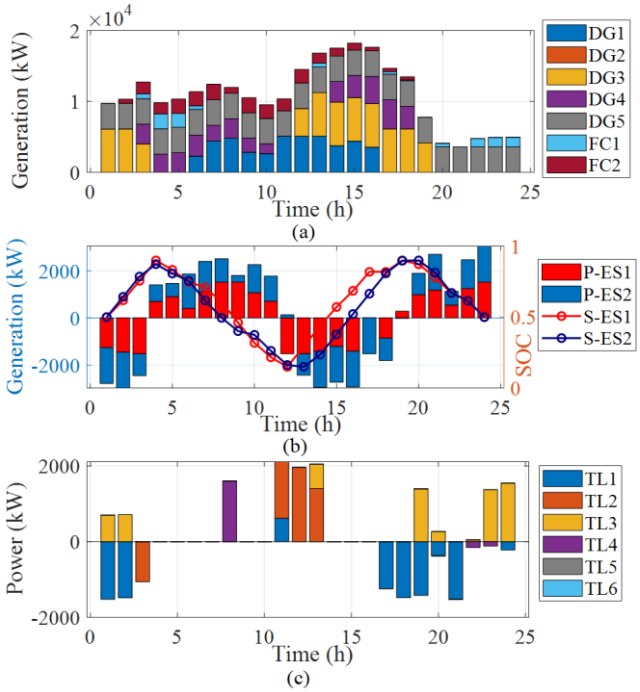

Figure 9. Outputs of the main units under the worst-case scenario (Case 2): (a) thermal power units; (b) ES units; (c) TLs.

In this case, the scheduling of greater thermal unit outputs is required, particularly for the DG5 in MG4 owing to its high industrial load. In fact, a comparison of Figs. 6(a) and 8(a) indicates that the power generation is greatly increased over the entire dispatch period relative to that observed for Case 1. Here, it is noted that Case 1 devotes to meeting the load balance constraint while avoiding the purchase of high-priced electricity from the main grid. Standby power requirements also encourage the scheduling of DGs to run continuously at low power outputs to meet unexpected decreases in RES outputs and unexpected increases in load demands. The impact of uncertainty is further demonstrated by the fact that the SOC curves of the two ESs are nearly equivalent in the worst-case scenario (Fig. 9(b)). This synchronization in the charge and discharge cycles of the ESs arises to ensure that the demands of the power systems are met, resulting in a decline in energy management flexibility. In addition, the fluctuation in the transmission power flow (Fig. 9(c)) is 17.18% greater under the worst-case scenario than that under the deterministic scenario, which also contributes to the higher operating cost.

In addition, the power flows and overall SOCs of the EVAs 1 are, respectively, given by the bar and line graphs presented in Fig. 10. Here, the values of UN, PI, and TP have already been shown in Fig. 8 with respect to Case 1 and are therefore not presented here. As illustrated in Figs. 11(a) and (b), we express the impact of unexpected changes in the energy storage capacity of EVAs in the worst-case scenario as a function of the actual and expected EV disconnection events of EVA1 and EVA2, respectively.

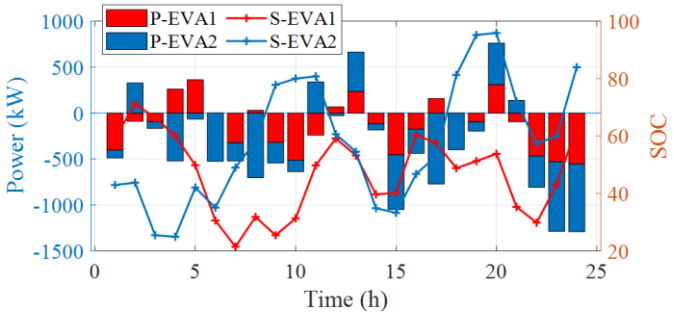

Figure 10. Scheduling solutions of EVAs under Case 2

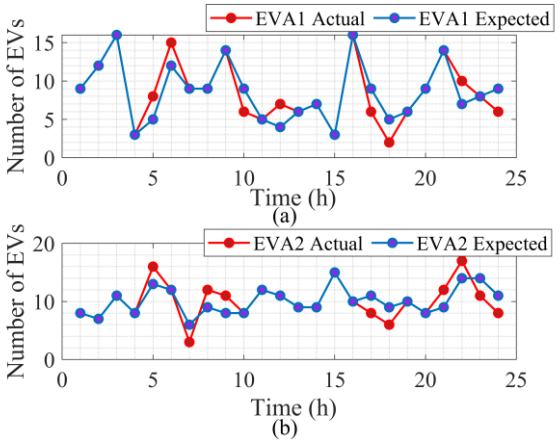

Figure 11. EV disconnection events in each period under Case 2: (a) EVA1; (b) EVA2.

It can be seen that there are some EVs accidentally disconnected from the power grid in actual scenario, which results in the difference between N_{UN} and N_{UN}^{*}. And for EVs disconnected in current scheduling cycle, the total size of upward and downward fluctuations is strictly equal, indicating the effectiveness of the proposed model. In other words, a more elaborated grid-interactive EVs model is presented by considering the multi-period coupling uncertainties of accidental disconnected EVs. Specifically. the accidental disconnections generally occur between 07:00–11:00 and 13:00–15:00 when the overall load increases quickly. This means that EVs disconnecting unexpectedly when operating in the V2G mode increase the up/down ramping rate requirements of the system, which is not economical. Even so, the EVAs were able to provide power to the local microgrids during low-load periods, which demonstrates the effectiveness and

economy of the robust V2G system. At the same time, the solution of the model satisfies the security scheduling constraints, which verifies the robustness and stability of the proposed model.

Case 3

The outputs of the thermal power and energy storage units obtained for various scenarios under Case 3 are presented as three-dimensional (3D) and 2D plots in Figs. 12(a) and (b), respectively. In addition, the transmission line power flows are presented in Fig. A1 in the appendix to limit the length of the article. We further note that the operating cost obtained for the convergent worst-case scenario set was 119288 yuan, which is 16.35% less than the operating cost obtained under Case 2 when using the conventional C&CG algorithm under the worst-case scenario. This is because ambiguity scenarios are constructed based on the distribution characteristics of historical scenario data to avoid theoretically existing but extreme scenarios, and therefore avoid overly conservative solutions.

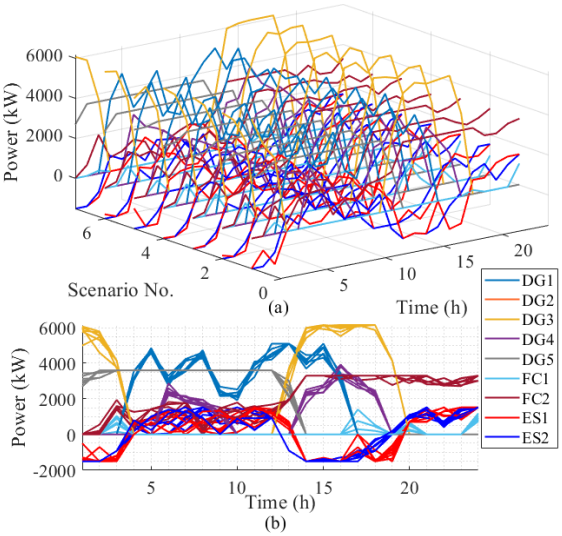

Figure 12. Outputs of the thermal and energy storage units for various scenarios under Case 3: (a) 3D plot; (b) 2D plot.

A comparison between Figs. 9 and 12 is made more convenient by plotting the outputs of the thermal power. The comparison indicates that the solution provided by Case 3 is similar to that provided by Case 2. We note from Fig. 12 and 6 that the outputs of most thermal power units, such as the power generation plans of FC1, FC2, and DG3, meet the variational characteristics of local loads. The scheduling schemes of ES1 and ES2 follow the standard feature of charging during periods of low load along with low electricity price and discharging during periods of high load and high electricity price. However, unlike being operational over the entire day period as observed under Case 2, DG5 is typically operational only from about 02:00 to about 12:00 over multiple scenarios in Case 3 to meet the power balance constraint. Again, this is because the ambiguity scenarios constructed based on the distribution characteristics of historical scenario data avoid theoretically existing but extreme scenarios.

More specifically, the normalized extreme distribution scenarios obtained based on the conventional DRO model are shown in Fig. 13, where L*i* is the *i*-th load power, E*i* is the number of EVs accidentally disconnected from EVA*i*, and S*x* represents scenario No. *x*. The results of data analysis demonstrate that some similarity is observable between the predicted scenario and the extreme distribution scenario.

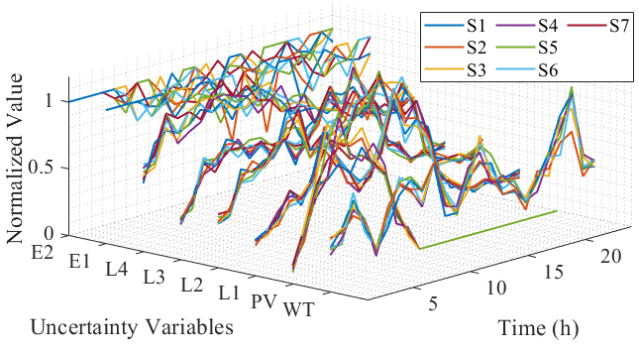

Figure 13. Distributions for main-unit outputs and loads under extreme scenarios for Case 3, where S*x* represents scenario No. *x*.

Case 4

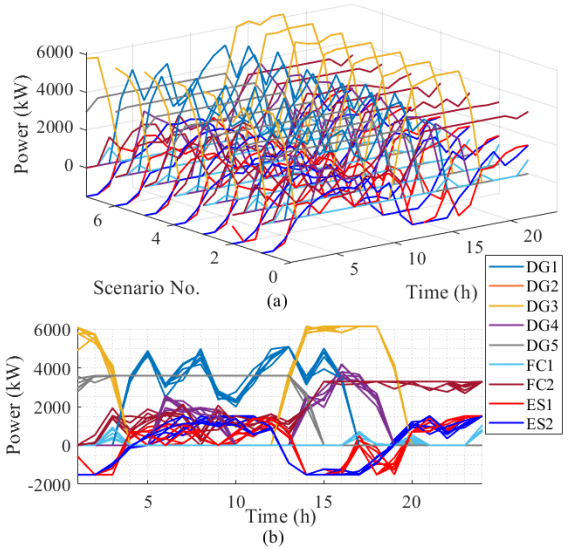

Figure 14. Outputs of the thermal and energy storage units for various scenarios under Case 4: (a) 3D plot; (b) 2D plot.

The outputs of the thermal power units and energy storage units obtained for various scenarios under Case 4 are presented as 3D and 2D plots in Figs. 14(a) and (b), respectively, and the transmission line power flows are presented in Fig. A2 in the appendix. In addition, the operating cost obtained for the convergent worst-case scenario was 120940 yuan, which is slightly greater than that obtained under Case 3 without applying the clustering method. At the same time, it is 15.19% less than that obtained under Case 2 using the conventional C&CG with the worst-case scenario.

A comparison between Figs. 12 and 14 indicates that the solution provided by Case 4 is similar to that provided by Case 3, and, according to the past discussion, is therefore similar to that provided by Case 2. The observed similarities verify the feasibility and stability of the KNN-based clustering method. Furthermore, the slightly greater operating cost under Case 4 than that under Case 3 indicates that the clustered scenario set ensures against worst-case scenarios better than the conventional scenario reduction method. We expect that the clustering process retains more features of the original scenario set than the simple scenario reduction method. Accordingly, the proposed approach is far more compatible with real-time scheduling operations that can be combined with short-term forecasts. It offers a much higher value in actual engineering applications than the simple scenario reduction method. Similarly, the normalized extreme distribution scenarios obtained based on the conventional DRO model are shown in Fig. 15.

In summary, the identical operating results of Case 1 under a deterministic scenario verified the feasibility of the proposed model, while the stability of the proposed solution method was demonstrated. Case 2 demonstrated that the EV aggregation mechanism effectively compensated for power deficits caused by renewable energy fluctuations under the worst-case scenario. Then, Case 3 demonstrated that the ambiguity scenarios constructed based on the distribution characteristics of historical scenario data avoided theoretically existing but extreme scenarios, and therefore avoided overly conservative solutions. Meanwhile, the results of Case 4 demonstrated that the proposed scenario clustering method can provide ambiguity sets with better robustness than the simple scenario reduction method employed in Case 3. Moreover, the clustering process is expected to retain more features of the original scenario set than the simple scenario reduction method.

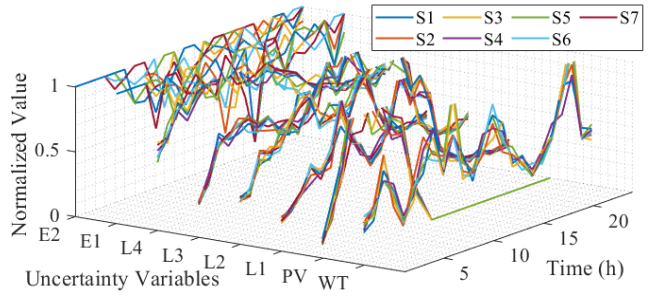

Figure 15. Distributions for main-unit outputs and loads under extreme scenarios for Case 4.

4.3 Benefits of EVA storage and convergence rates

The extent of RES consumption under extreme scenarios was evaluated by adding the penalty coefficients to the objective function of the optimization models in Cases 1–4. Here, it should be noted that the determination of penalty coefficients affects the abandonment of wind and solar energy and load shedding. We also introduced two nonnegative relaxation variables in each equality constraint to expand the region for which feasible solutions can be obtained under the four test cases. Here, the solution process is allowed to converge naturally if the relaxation variables remain 0, while the equality constraint is relaxed if the value of the relaxation variable is greater than 0. By the inclusion of V2G service and the setting of reasonable penalty coefficients in the objective function, the results obtained under all Cases show that the quantities of wind and solar energy abandonment, load shedding, and required slack electric power were uniformly 0 kWh.

The convergence of the solution processes observed under Cases 1–4 by comparing the upper bound (UB) and lower bound (LB) operational costs obtained at each iteration was less than 0.1%. The results are listed in Table 4, which shows stable convergence in all cases. The deterministic scenario under Case 1 had shortest convergence time, while the C&CG algorithm produced the largest error in the first iteration for Cases 2–4. This was due to the large number of EVs included in the model, which increases the operational constraints of the MP, and greatly increases the number of vertices of the polyhedron uncertainty set. As a result, reducing number of scenarios applied in Cases 3 and 4 successively reduced the error observed in the first iteration. This suggests that these methods progressively increase the robustness of the scenario set and improve the convergence performance of the model continuously.

Table 4. Information regarding the four case studies employed for testing

Cost (yuan) \ Iteration	1	2	3
Case 1-LB	118418		
Case 1-UB	118418		
Error	0		
Case 2-LB	118418	142596	
Case 2-UB	1879716	142597	
Error	1487.3 %	0.01%	
Case 3-LB	118418	119288	
Case 3-UB	828909	119323	
Error	599.98 %	0.03 %	
Case 4-LB	118418	120940	
Case 4-UB	398588	121013	
Error	236.59%	0.06%	

On the other hand, as a key parameter, the number of selected scenarios needs to be determined based on the number of historical scenarios as well as the operating performance of the EMS platform. Accordingly, as shown in Fig. 16, the expectation cost and convergence time of cases with different number of scenarios N_s are presented.

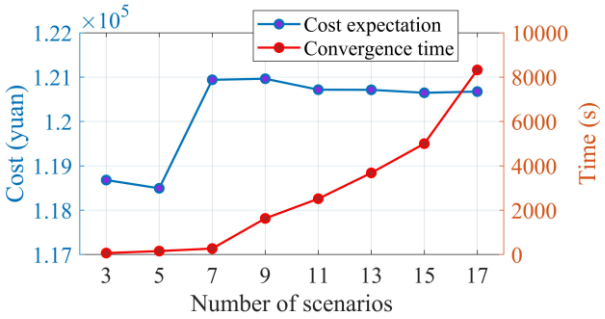

Figure 16. Comparison of computational performance between different N_s Cases.

It should be noted that cost expectation of cases with N_s greater than or equal to 7 is very similar, with only a slight difference (< 0.2 %) due to the random initialization of the weights in the KNN clustering process. This suggests that the N_s = 7 selected in this paper is sufficient to represent the robustness of historical data and to obtain operation results with a reasonable convergence time.

4.4 Security benefits of cross-cycle SOCs continuity

To verify the effectiveness of the proposed model for cross-cycle robust operation, this subsection compares the optimization results with and without considering the cross-cycle SOCs continuity. Table 5 shows the cost, the initial energy $I_{E,i}$ and slack powers requirement $R_{x,i}$ of EVAi for different cases, where Ci" denotes the Case i with the proposed model, and Ci denotes the Case i with the conventional model.

Table 5. Comparison of operating results between different cases

	Cost (yuan)	$R_{x,1}$ (kWh)	$R_{x,2}$ (kWh)	$I_{E,1}$ (kWh)	$I_{E,2}$ (kWh)
C2"	142596	0	0	1306	946
C3"	119288				
C4"	120940				
C2	167008	138	123	409	382
C3	143066				
C4	145124				

It can be seen that $R_{x,1}$ and $R_{x,2}$ are zero in C2", C3" and C4", while they are equal to 138 kWh and 123 kWh in C2, C3 and C4, respectively. This means that slack powers are redundant in the first three cases, while they are required in last three cases to ensure the feasible operation of the MMG. It is also observed from $I_{E,1}$ and $I_{E,2}$ that due to neglecting the SOC continuity of cross-cycle model, the SOC status of EVs still connected at the initial time period of the scheduling cycle are at a low level. In this regard, the neglection of cross-cycle SOCs continuity will affect the operation plan of the whole scheduling cycle, and even lead to the emergence of relaxation energy, posing a challenge to the security of the system.

More specifically, Fig. 16 shows the temporal costs of different cases. It is found that the operating costs of C2, C3 and C4 are significantly higher in the earlier time periods, suggesting that emergency measures are taken to prevent the power violations during the time periods that spanned the scheduling cycles. Meanwhile, when considering the cross-cycle model proposed in this paper, the slack powers in the coming scheduling cycle can be effectively avoided. Accordingly, a more efficient dispatch solution for grid-interactive EVs can be deployed by EMS to accommodate the uncertainties of RESs.

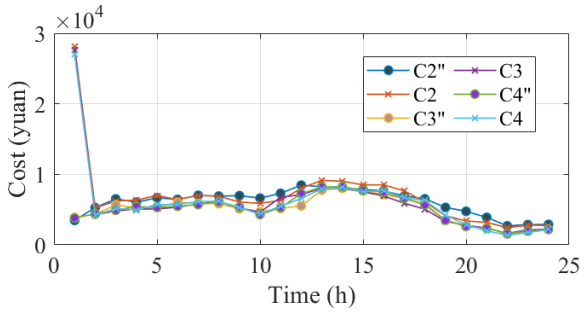

Figure 17. Temporal costs of different cases

V. Conclusion

The present work proposes a two-stage distributionally robust energy management model for the multi-microgrids that considers the grid-interactive EVs to accommodate uncertainties in RES outputs and local loads. Case studies are carried out on the system composed of four interconnected microgrid from Hainan provincial power grid. The results verify the superiority of the proposed model in terms of its convergence performance, cost efficiency, and robustness. Based on this work, the following conclusions can be drawn:

- The proposed distributionally robust energy management model for MMGs effectively explores the flexibility of grid-interactive EVs to accommodate the uncertainty of RESs, which can hedge against the worst-case distribution of random variables. Thus, a better tradeoff between cost efficiency and robustness can be made.
- The multi-period coupling effect of user behaviors including the cross-cycle continuity of SOCs and multi-period coupling uncertainties of accidental EVs disconnections are taken into account in this paper, which provides a more accurate EVA model for robust energy management.
- The proposed KNN-based ambiguity set can preserve the features of the entire scenario set by means of the representative scenarios and their weight, which greatly improves the convergence performance of the model solution.

However, the current work considered only the uncertainty associated with V2G-connected EV users accidentally disconnecting from the network. Future work will seek to improve the utility of the model further by establishing a hybrid optimization model considering the effect of EV aggregation on road networks and power grids.

Acknowledgments

This work was supported by the Innovation and Technology Fund (ITP/002/22LP) of the Hong Kong SAR, the RISUD of The Hong Kong Polytechnic University (Project No. P0042845) and the National Key Research and Development Program of China (2022YFB2403500).

References

[1] Kennedy KM, Ruggles TH, Rinaldi K, Dowling JA, Duan L, Caldeira K, et al. The role of concentrated solar power with thermal energy storage in least-cost highly reliable electricity systems fully powered by variable renewable energy. Advances in Applied Energy 2022;6:100091. https://doi.org/10.1016/j.adapen.2022.100091.

[2] Hong B, Zhang W, Zhou Y, Chen J, Xiang Y, Mu Y. Energy-Internet-oriented microgrid energy management system architecture and its application in China. Applied Energy 2018;228:2153–64. https://doi.org/10.1016/j.apenergy.2018.07.081.

[3] Liang Z, Chen H, Wang X, Chen S, Zhang C. Risk-Based Uncertainty Set Optimization Method for Energy Management of Hybrid AC/DC Microgrids With Uncertain Renewable Generation. IEEE Trans Smart Grid 2020;11:1526–42. https://doi.org/10.1109/TSG.2019.2939817.

[4] Polimeni S, Meraldi L, Moretti L, Leva S, Manzolini G. Development and experimental validation of hierarchical energy management system based on stochastic model predictive control for Off-grid Microgrids. Advances in Applied Energy 2021;2:100028. https://doi.org/10.1016/j.adapen.2021.100028.

[5] Peddakapu K, Srinivasarao P, Mohamed MR, Arya Y, Krishna Kishore DJ. Stabilization of frequency in Multi-Microgrid system using barnacle mating Optimizer-based cascade controllers. Sustainable Energy Technologies and Assessments 2022;54:102823. https://doi.org/10.1016/j.seta.2022.102823.

[6] Dong Z, Zhang X, Zhang N, Kang C, Strbac G. A distributed robust control strategy for electric vehicles to enhance resilience in urban energy systems. Advances in Applied Energy 2023;9:100115. https://doi.org/10.1016/j.adapen.2022.100115.

[7] Borozan S, Giannelos S, Strbac G. Strategic network expansion planning with electric vehicle smart charging concepts as investment options. Advances in Applied Energy 2022;5:100077. https://doi.org/10.1016/j.adapen.2021.100077.

[8] Gilleran M, Bonnema E, Woods J, Mishra P, Doebber I, Hunter C, et al. Impact of electric vehicle charging on the power demand of retail buildings. Advances in Applied Energy 2021;4:100062. https://doi.org/10.1016/j.adapen.2021.100062.

[9] Soykan G, Er G, Canakoglu E. Optimal sizing of an isolated microgrid with electric vehicles using stochastic programming. Sustainable Energy, Grids and Networks 2022;32:100850. https://doi.org/10.1016/j.segan.2022.100850.

[10] Abunima H, Park W-H, Glick MB, Kim Y-S. Two-Stage stochastic optimization for operating a Renewable-Based Microgrid. Applied Energy 2022;325:119848. https://doi.org/10.1016/j.apenergy.2022.119848.

[11] Bagheri F, Dagdougui H, Gendreau M. Stochastic optimization and scenario generation for peak load shaving in Smart District microgrid: sizing and operation. Energy and Buildings 2022;275:112426. https://doi.org/10.1016/j.enbuild.2022.112426.

[12] Guo S, Li P, Ma K, Yang B, Yang J. Robust energy management for

industrial microgrid considering charging and discharging pressure of electric vehicles. Applied Energy 2022;325:119846. https://doi.org/10.1016/j.apenergy.2022.119846.

[13] Cheng Z, Jia D, Li Z, Si J, Xu S. Multi-time scale dynamic robust optimal scheduling of CCHP microgrid based on rolling optimization. International Journal of Electrical Power & Energy Systems 2022;139:107957. https://doi.org/10.1016/j.ijepes.2022.107957.

[14] Hani Gilani, Hadi Sahebi, Mir Saman Pishvaee, A data-driven robust optimization model for integrated network design solar photovoltaic to micro grid, Sustainable Energy, Grids and Networks, Volume 31, 2022, 100714, https://doi.org/10.1016/j.segan.2022.100714.

[15] Zandrazavi SF, Guzman CP, Pozos AT, Quiros-Tortos J, Franco JF. Stochastic multi-objective optimal energy management of grid-connected unbalanced microgrids with renewable energy generation and plug-in electric vehicles. Energy 2022;241:122884. https://doi.org/10.1016/j.energy.2021.122884.

[16] Li X, Liu Y, Li G, Li X, Wang C. A data-driven based uncertainty set modelling method for microgrid robust optimization with correlated wind power. CSEE Journal of Power and Energy Systems 2022:1–12. https://doi.org/10.17775/CSEEJPES.2021.06330.

[17] Zhu C, Wang L, Huang J, Cheng H, Hou G, Zhang S, Liu H, Feasibility analysis of PV and energy storage system integration for flexible distribution networks: A moment-based distributionally robust approach, Energy Reports, Volume 9, Supplement 3, 2023, Pages 89-98, https://doi.org/10.1016/j.egyr.2022.12.099.

[18] Zheng X, Chen H. Data-Driven Distributionally Robust Unit Commitment With Wasserstein Metric: Tractable Formulation and Efficient Solution Method. IEEE Trans Power Syst 2020;35:4940–3. https://doi.org/10.1109/TPWRS.2020.3014808.

[19] Xu Y-P, Liu R-H, Tang L-Y, Wu H, She C. Risk-averse multi-objective optimization of multi-energy microgrids integrated with power-to-hydrogen technology, electric vehicles and data center under a hybrid robust-stochastic technique. Sustainable Cities and Society 2022;79:103699. https://doi.org/10.1016/j.scs.2022.103699.

[20] Cao Y, Li D, Zhang Y, Tang Q, Khodaei A, Zhang H, et al. Optimal Energy Management for Multi-Microgrid Under a Transactive Energy Framework With Distributionally Robust Optimization. IEEE Trans Smart Grid 2022;13:599–612. https://doi.org/10.1109/TSG.2021.3113573.

[21] Li Z, Wu L, Xu Y, Zheng X. Stochastic-Weighted Robust Optimization Based Bilayer Operation of a Multi-Energy Building Microgrid Considering Practical Thermal Loads and Battery Degradation. IEEE Trans Sustain Energy 2022;13:668–82. https://doi.org/10.1109/TSTE.2021.3126776.

[22] Shi R, Li S, Zhang P, Lee KY. Integration of renewable energy sources and electric vehicles in V2G network with adjustable robust optimization. Renewable Energy 2020;153:1067–80. https://doi.org/10.1016/j.renene.2020.02.027.

[23] Zhang X, Wang Z, Lu Z. Multi-objective load dispatch for microgrid with electric vehicles using modified gravitational search and particle swarm optimization algorithm. Applied Energy 2022;306:118018. https://doi.org/10.1016/j.apenergy.2021.118018.

[24] Zare Ghaleh Seyyedi A, Akbari E, Atazadegan MH, Mahmoudi Rashid S, Niazazari A, Shahmoradi S. A stochastic tri-layer optimization framework for day-ahead scheduling of microgrids using cooperative game theory approach in the presence of electric vehicles. Journal of Energy Storage 2022;52:104719. https://doi.org/10.1016/j.est.2022.104719.

[25] Wu C, Gao S, Liu Y, Song TE, Han H. A model predictive control approach in microgrid considering multi-uncertainty of electric vehicles. Renewable Energy 2021;163:1385–96. https://doi.org/10.1016/j.renene.2020.08.137.

[26] Dai S, Gao F, Guan X, Yan C-B, Liu K, Dong J, et al. Robust Energy Management for a Corporate Energy System With Shift-Working V2G. IEEE Trans Automat Sci Eng 2021;18:650–67. https://doi.org/10.1109/TASE.2020.2980356.

[27] Tan B, Chen H, Zheng X, Huang J. Two-stage robust optimization dispatch for multiple microgrids with electric vehicle loads based on a novel data-driven uncertainty set. International Journal of Electrical Power & Energy Systems 2022;134:107359. https://doi.org/10.1016/j.ijepes.2021.107359.

[28] Li Z, Wu L, Xu Y, Wang L, Yang N, Distributed tri-layer risk-averse stochastic game approach for energy trading among multi-energy microgrids, Applied Energy, Volume 331, 2023, 120282, https://doi.org/10.1016/j.apenergy.2022.120282.

[29] Huang H, Li Z, Hoay Beng Gooi, Haifeng Qiu, Xiaotong Zhang, Chaoxian Lv, Rui Liang, Dunwei Gong, Distributionally robust energy-transportation coordination in coal mine integrated energy systems, Applied Energy, Volume 333, 2023, 120577, https://doi.org/10.1016/j.apenergy.2022.120577.

[30] Yuan Z, Li P, Li Z, Xia J. Data-Driven Risk-Adjusted Robust Energy Management for Microgrids Integrating Demand Response Aggregator and Renewable Energies. IEEE Trans Smart Grid 2023;14:365–77. https://doi.org/10.1109/TSG.2022.3193226.

[31] Z. Li, Y. Xu, S. Fang, X. Zheng and X. Feng, "Robust Coordination of a Hybrid AC/DC Multi-Energy Ship Microgrid With Flexible Voyage and Thermal Loads," in IEEE Transactions on Smart Grid, vol. 11, no. 4, pp. 2782-2793, July 2020, doi: 10.1109/TSG.2020.2964831.

[32] Kalpathy Jayanth Krishnan, Kishalay Mitra, A modified Kohonen map algorithm for clustering time series data, Expert Systems with Applications, Volume 201, 2022, 117249, https://doi.org/10.1016/j.eswa.2022.117249.

[33] Hemanth DJ, Anitha J, Son LH. Brain signal based human emotion analysis by circular back propagation and Deep Kohonen Neural Networks. Computers & Electrical Engineering 2018;68:170–80. https://doi.org/10.1016/j.compeleceng.2018.04.006.

[34] Singh A, Quek C, Cho S-Y. DCT-Yager FNN: A Novel Yager-Based Fuzzy Neural Network With the Discrete Clustering Technique. IEEE Trans Neural Netw 2008;19:625–44. https://doi.org/10.1109/TNN.2007.911709.

[35] Chen H, Xuan P, Wang Y, Tan K, Jin X. Key Technologies for Integration of Multitype Renewable Energy Sources—Research on Multi-Timeframe Robust Scheduling/Dispatch. IEEE Trans Smart Grid 2016;7:471–80. https://doi.org/10.1109/TSG.2015.2388756.

[36] Wang L, Zhang B, Li Q, Song W, Li G. Robust distributed optimization for energy dispatch of multi-stakeholder multiple microgrids under uncertainty. Applied Energy 2019;255:113845. https://doi.org/10.1016/j.apenergy.2019.113845.

[37] Li Z, Xu Y. Temporally-coordinated optimal operation of a multi-energy microgrid under diverse uncertainties. Applied Energy 2019;240:719–29. https://doi.org/10.1016/j.apenergy.2019.02.085.

[38] Forget N, Gadegaard SL, Klamroth K, Nielsen LR, Przybylski A. Branch-and-bound and objective branching with three or more objectives. Computers & Operations Research 2022;148:106012. https://doi.org/10.1016/j.cor.2022.106012.

Appendix

1. Simulations results of the transmission lines

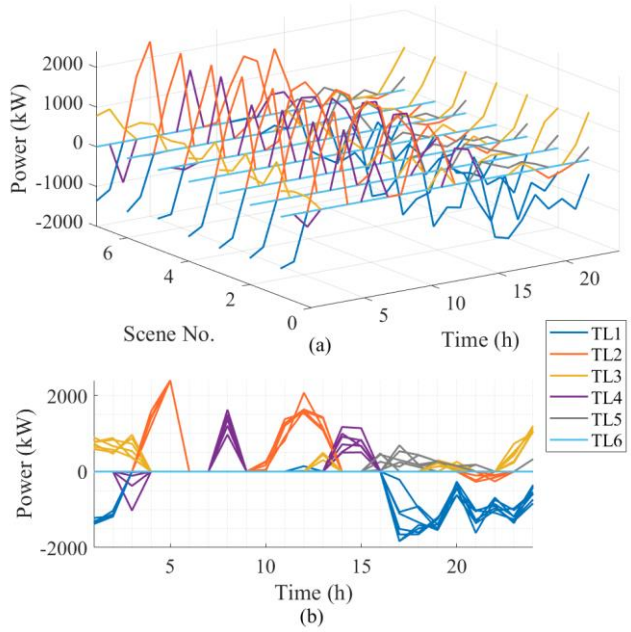

Figure A1. Outputs of the transmission lines for various scenarios under Case 3: (a) 3D plot; (b) 2D plot.

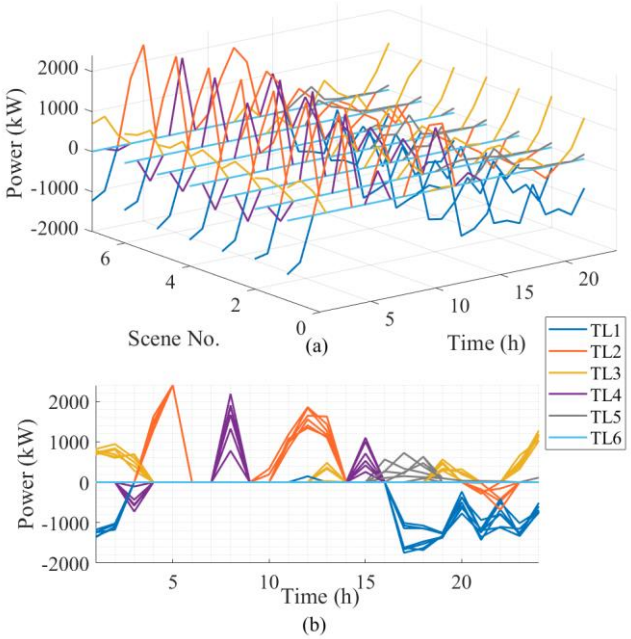

Figure A2. Outputs of the transmission lines for various scenarios under Case 4: (a) 3D plot; (b) 2D plot